

The role of slab geometry in the exhumation of cordilleran-type orogens and their forelands: Insights from northern Patagonia

Marie C. Genge^{1,2}, Massimiliano Zattin¹, Elisa Savignano¹, Marta Franchini^{3,4}, Cécile Gautheron⁵, Victor A. Ramos⁶, and Stefano Mazzoli^{7,†}

¹Department of Geosciences, University of Padua, Italy

²Université de Lille, CNRS, Université du Littoral—Côte d'Opale, UMR 8187, LOG, Laboratoire d'Océanologie et de Géosciences, F 59000 Lille, France

³Instituto de Investigación en Paleobiología y Geología, Universidad Nacional de Río Negro, Argentina

⁴Centro Patagónico de Estudios Metalogénicos, Universidad Nacional del Comahue, Neuquén, Argentina

⁵GEOPS, Université Paris Sud, CNRS, Université Paris-Saclay, Orsay, France

⁶Instituto de Estudios Andinos, UBA-CONICET, Buenos Aires, Argentina

⁷School of Sciences and Technology, Geology Division, University of Camerino, Italy

ABSTRACT

In cordilleran-type orogens, subduction geometry exerts a fundamental control on the tectonic behavior of the overriding plate. An integrated low-temperature, large thermochronological data set is used in this study to investigate the burial and exhumation history of the overriding plate in northern Patagonia (40°–45°S). Thermal inverse modeling allowed us to establish that a ~2.5–4-km-thick section originally overlaid the Jurassic–Lower Cretaceous successions deposited in half-graben systems that are presently exposed in the foreland. Removal of the sedimentary cover started in the late Early Cretaceous. This was coeval with an increase of the convergence rate and a switch to a westward absolute motion of the South American Plate that was accompanied by shallowing of the subducting slab. Unroofing was probably further enhanced by Late Cretaceous to early Paleogene opening of a slab window beneath the overriding plate. Following a tectonically quiescent period, renewed exhumation occurred in the orogen during relatively fast Neogene plate convergence. However, even the highly sensitive apatite (U-Th)/He thermochronometer does not record any coeval cooling in the foreland. The comparison between Late Cretaceous and Neogene exhumation patterns provides clear evidence of the fundamental role played by inter-plate coupling associated with shallow slab configurations in controlling plate-scale

deformation. Our results, besides highlighting for the first time how the whole northern Patagonia foreland was affected by an exhumation of several kilometers since the Late Cretaceous, provide unrivalled evidence of the link between deep geodynamic processes affecting the slab and the modes and timing of unroofing of different sectors of the overriding plate.

INTRODUCTION

Mechanical plate coupling is governed by subduction geometry and particularly by slab dip. This latter is controlled by various parameters including: (1) upper plate absolute motion, (2) subducting slab buoyancy, (3) overriding plate temperature, and (4) faulting of the oceanic lithosphere (Gutscher, 2002; Gutscher and Peacock, 2003; Lallemand et al., 2005; Rodríguez-González et al., 2012; Cerpa et al., 2018). Many authors also pointed out correlations in time and space between shallow slab segments and the subduction of buoyant oceanic features such as aseismic ridges or oceanic plateau (Pilger, 1981; McGeary et al., 1985; Gutscher et al., 2000). Upper plate compression is generally associated with strong interplate coupling during shallow to flat-slab subduction, while extension is correlated with weak interplate coupling during slab rollback. Therefore, plate-coupling variations are believed to result in alternating phases of upper plate shortening and extension (Lallemand et al., 2005; Horton, 2018), thereby regulating orogenic growth and foreland evolution (Martinod et al., 2010). Although a high degree of interplate coupling can also characterize steep subduction (depending on convergence rate), this is gener-

ally less effective with respect to that associated with shallow to flat-slab segments (Gutscher, 2002). At present, slab dip varies significantly along the Andean margin from the dominant dip angle of ~30° to flat-slab segments (Ramos and Folguera, 2009; Horton and Fuentes, 2016; Maksymowicz and Tassara, 2018). This results in along-strike segmentation and coupling variations that influence magmatism and the style of recent to active deformation of the overriding plate (Coira et al., 1993; Yáñez and Cembrano, 2004; Ramos and Folguera, 2009).

The geological record of pulsed, upper plate shortening episodes in Patagonia has been related to variable plate coupling associated with changes of plate convergence settings and particularly slab dip (Echaurren et al., 2016; Gianni et al., 2015; Horton, 2018; Orts et al., 2012). Two orogenic stages, a late Early Cretaceous to early Paleogene stage and a middle Miocene to Pliocene stage, have been recognized in the Patagonian Cordillera, the Patagonian Precordillera (Fig. 1A; also named the Precordilleran system, or the Eastern Precordillera, or the North Patagonian fold and thrust belt; e.g., Bilmes et al., 2013; Folguera et al., 2018; Orts et al., 2015; Ramos et al., 2014), and the so-called broken foreland generated by the uplift of basement blocks related to the contractional reactivation of older crustal discontinuities and the deformation of former graben/half graben systems (Echaurren et al., 2016; López et al., 2019). These latter were formed in the context of Early Jurassic to Early Cretaceous extension associated with a protracted slab rollback, which is coherent with the westward shift of arc magmatism (Ramos, 1999, 2010). Similar processes have been documented for the intervening late

†Corresponding author: stefano.mazzoli@unicam.it.

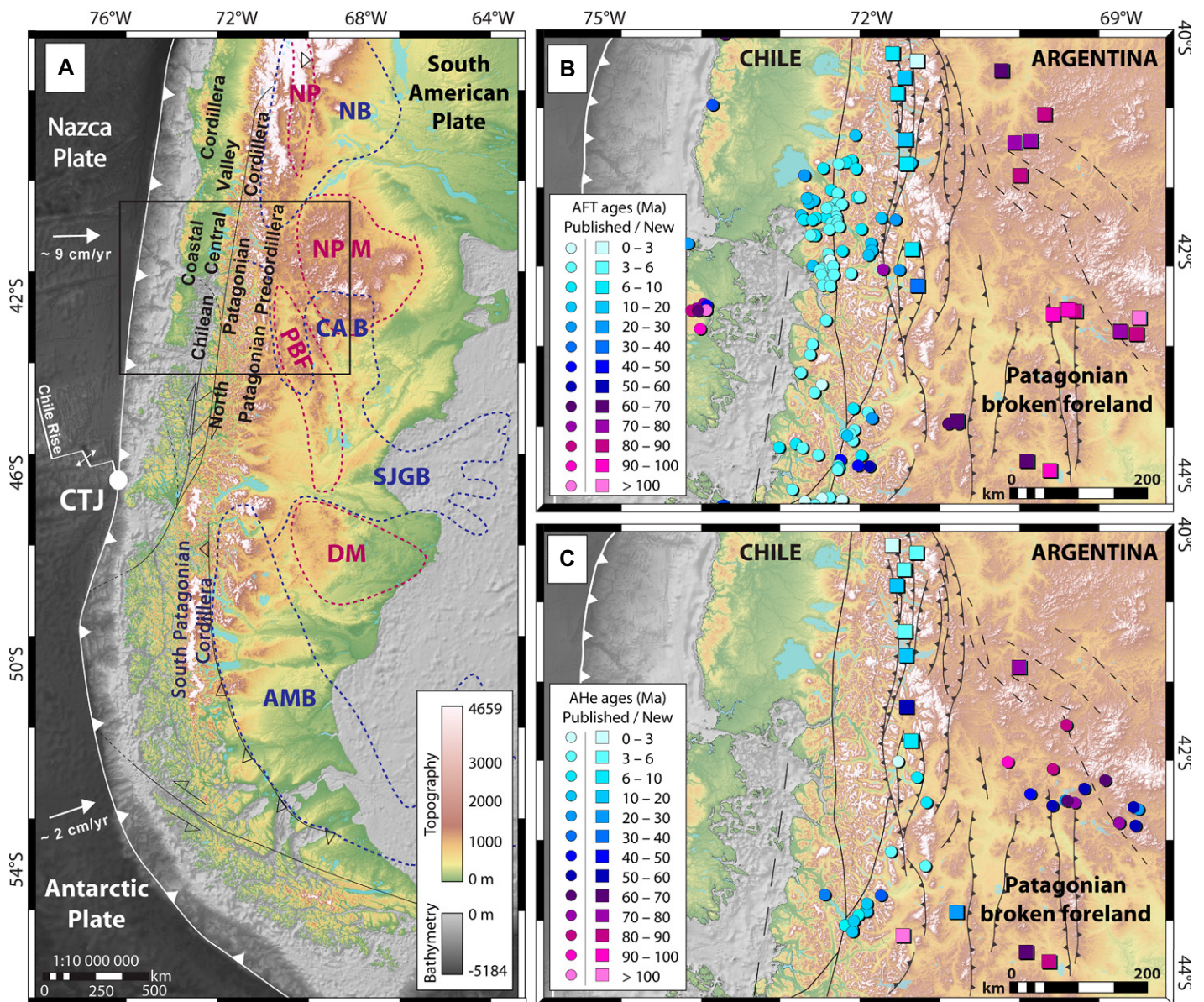


Figure 1. (A) Map view of major tectonic features of the Southern Andes (modified after Navarrete et al., 2016) shows locations of diagrams B–C. Blue dashed lines outline foreland basins (AMB—Austral-Magallanes Basin, CAB—Cañadón Asfalto Basin, NB—Neuquén Basin, and SJGB—San Jorge Gulf Basin); purple dashed lines outline foreland reliefs (DM—Deseado Massif, NPM—North Patagonian Massif, NP—Neuquén Precordillera, and PBF—Patagonian broken foreland). White arrows indicate current motions of oceanic plates relative to South America according to the global model NUVEL-1. **(B)** Map view of main morphotectonic features between 40°S and 45°S with new and published (Thomson, 2002; Thomson et al., 2010) apatite fission track (AFT) ages. **(C)** New and published (Thomson et al., 2010; Savignano et al., 2016) apatite (U-Th)/He (AHe) ages.

Eocene to early Miocene period, characterized by abundant magmatism toward the Cordillera and modest foreland subsidence (Folguera and Ramos, 2011; Horton, 2018). The localization of deformation in former basins emphasizes the role of inherited upper plate weaknesses in controlling the propagation of the deformation to the broken foreland during regional shortening episodes (Gianni et al., 2017). However, little is known about the amount of regional unroofing in the foreland of the Patagonian Andes, as

thermochronological studies focused mainly on the growth of the Cordillera (Thomson et al., 2010). In this study we present the results obtained by thermal inverse modeling of low-temperature thermochronology data collected in the Patagonian Cordillera and the broken foreland between 40°S and 45°S (Figs. 1B and 1C) with the goal of evaluating the impact of slab geometry changes—and associated plate coupling variations—on the deformation of the overriding plate. Our results provide a new and

unexpected picture of the large unroofing (in excess of 3 km considering an average geothermal gradient of $\sim 34 \pm 11^\circ\text{C}/\text{km}$) experienced by the whole northern Patagonia foreland—and not just the Cordillera—since the late Early Cretaceous.

GEOLOGICAL SETTING

The northern Patagonian margin is characterized by several morphotectonic units, including the Patagonian Precordillera and the

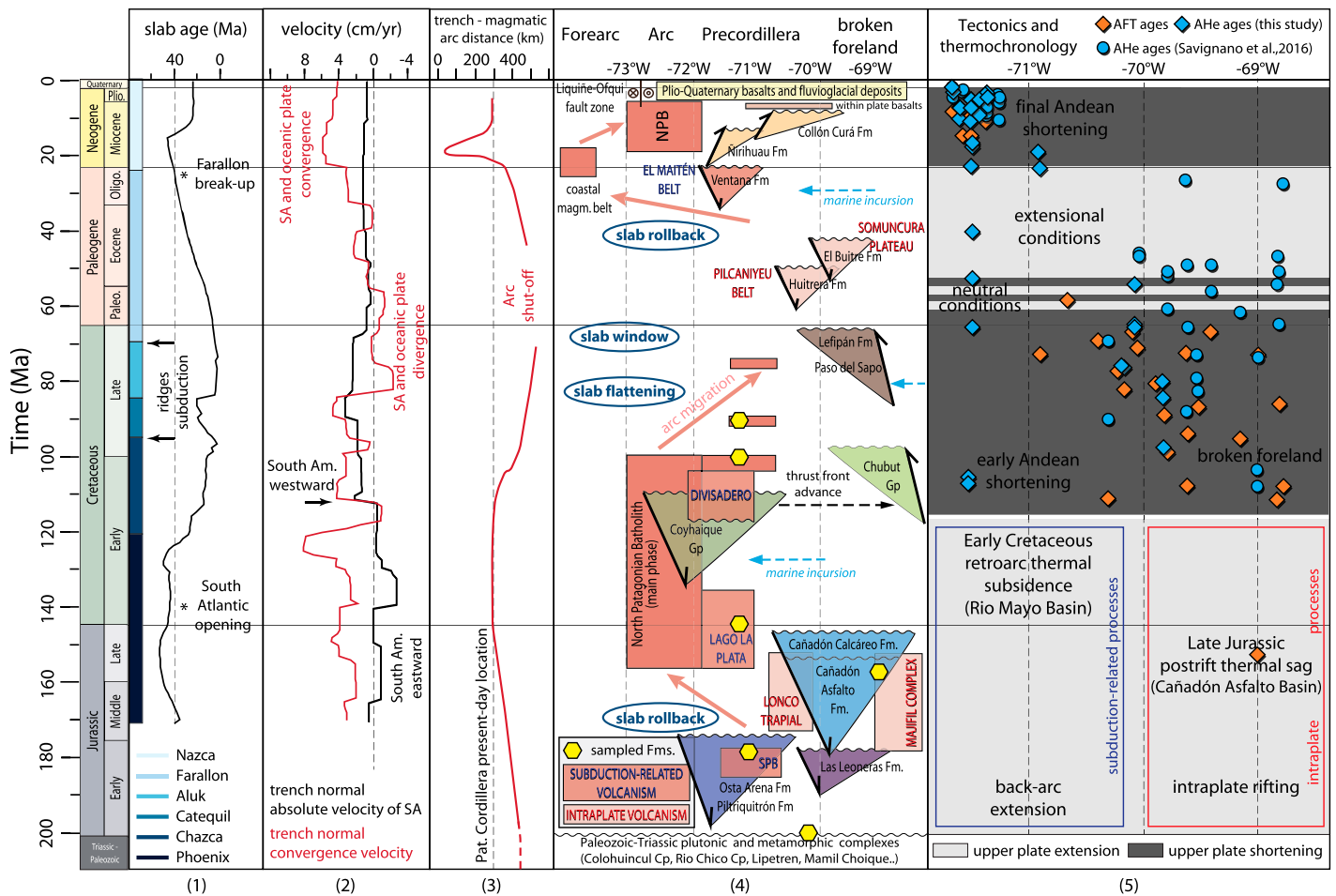


Figure 2. Chronological table for northern Patagonia at around 43°S shows from left to right columns: (1) oceanic plates subducting beneath South America at this latitude through time and slab age (Maloney et al., 2013); (2) plate convergence rate (note the change of the South American Plate motion to the west during the Early Cretaceous as well as periods of plate convergence and divergence; modified from Maloney et al. (2013); (3) distance between the magmatic arc and the trench, which is considered to be a fixed reference marker. Note trenchward migration due to slab rollback during the entire Jurassic and the Oligocene–early Miocene time span and migration toward the eastern foreland during the Late Cretaceous and the middle–late Miocene as well as period of arc shut-off; modified after Gianni et al. (2018); (4) time-space evolution of the magmatic arc and basin development with the different sedimentary and magmatic formations identified in the studied area (note magmatic arc migration toward either the trench or the eastern foreland during slab steepening or slab shallowing episodes, respectively; Echaurren et al., 2016; Horton, 2018; Butler et al., 2020); and (5) the thermochronological data (apatite fission track and apatite (U-Th)/He ages versus longitudinal distribution) used in this study with the time-space evolution of deformation according to Horton (2018) and Butler et al. (2020).

broken foreland to the east (Fig. 1A; Echaurren et al., 2016). The Precordillera is a retro-arc thick-skinned fold-thrust belt (Giacosa and Heredia, 2004; Orts et al., 2012). On the other hand, the broken foreland got its name because it is structurally articulated and fragmented by a series of uplifted blocks (e.g., Bilmes et al., 2013). Regional deformation in northern Patagonia is characterized by the shortening of former sedimentary basins (Piltriquitrón Basin and Rio Mayo Basin along the Precordillera, Cañadón Asfalto Rift Basin to the foreland) that developed on top of a low-grade metamorphic basement. The latter is constituted of Paleozoic-

Triassic, volcano-sedimentary successions (e.g., Cushamen, Calcatapul Formations; Volkheimer, 1964; von Gosen and Loske, 2004) and coeval intrusions (e.g., Colohuincul Complex, Mamil Choique, and Lipetrén Formations; Rapela et al., 1992; Ravazzoli and Sesana, 1977; Turner, 1965; Varela et al., 2005). The Cañadón Asfalto Rift Basin is mainly the product of extension induced by Gondwana break-up during the Early Jurassic and of the following Early Cretaceous sag stage (Fig. 2; Figari et al., 2015; Mpodozis and Ramos, 2008). The sedimentary infill includes the continental Las Leoneras Formation, followed above by the Cañadón Asfalto and Cañadón

Calcáreo Formations, which are laterally interbedded with the volcanic Lonco Trapial Formation (Zaffarana and Somoza, 2012; Cúneo et al., 2013). Few discordances observed in the basin succession are correlated with minor shortening events associated with changes in plate motion and volcanic activity (Maloney et al., 2013; Figari et al., 2015; Navarrete et al., 2016, 2018). Along the Patagonian Precordillera, roughly coeval back-arc extension was triggered by a protracted slab rollback generated by low convergence rates and eastward motion of the South American Plate (Giacosa and Heredia, 2004; Suarez and Marquez, 2007; Seton et al., 2012;

Maloney et al., 2013; Horton, 2018). This resulted in steepening of the slab, as evidenced by the westward migration of the magmatic arc (Fig. 2) marked by the Lower Jurassic Subcordillera Plutonic Belt (Gordon and Ort, 1993; Page and Page, 1999) and by the Upper Jurassic–Lower Cretaceous North Patagonian Batholith (Suárez and De la Cruz, 2001; Pankhurst et al., 2003). Indeed, lateral shifts of the magmatic arc either toward the trench or toward the eastern foreland are promoted by variations of the subduction zone configuration involving slab steepening or shallowing episodes, respectively (e.g., Coira et al., 1993; England et al., 2004; Kay et al., 2005; Ramos and Folguera, 2005; Syracuse and Abers, 2006; Folguera and Ramos, 2011; Spagnuolo et al., 2012; Schellart, 2017; Fernández Paz et al., 2019).

Coeval volcanism is recorded by the Middle–Upper Jurassic Lago La Plata Formation (correlated with the Ibáñez Group in Chile; Folguera and Iannizzotto, 2004; Olivero, 1982) and the Lower Cretaceous Divisadero Group (Ramos, 1981; Suárez et al., 2009). Respectively, these volcanic deposits overlie the N–NE–trending, graben/half-graben systems of the Piltriquitrón Basin (filled by the Lower–Middle Jurassic Osta Arena Formation, Piltriquitrón Formation, and equivalent units intercalated with marine successions; Gabaldón, 1982; Giacosa and Heredia, 2004; Suarez and Marquez, 2007), and the Upper Jurassic–Lower Cretaceous sedimentary successions of the Coyhaique Group hosted in the Rio Mayo Basin (Skarmeta, 1976; Olivero, 1982; Echaurren et al., 2017). As revealed by the regional unconformity observed in the upper volcanic succession of the Divisadero Group and on top of the Cañadón Asfalto Rift Basin deposits, extension was suddenly interrupted at ca. 120 Ma by a regional shortening episode (Folguera and Iannizzotto, 2004; Suárez et al., 2009; Horton, 2018). This latter, acting on a continental crust mechanically weakened by faults, produced both the earliest stage of Andean uplift and deformation of the Patagonian broken foreland. Indeed, the deformation, reaching areas ~500 km away from the trench (Navarrete et al., 2016), was dominated by the reactivation of existing faults associated with the shortening of former depocenters (Gianni et al., 2015). The initiation of regional shortening coincided with a change of absolute motion of the South American Plate, which became west directed (Fig. 2; Maloney et al., 2013; Müller et al., 2016; Seton et al., 2012; Silver et al., 1998). Trenchward absolute motion of the overriding plate and an increase of convergence rates (Eagles, 2007; Maloney et al., 2013; Müller et al., 2016) were accompanied by slab shallowing manifested in the upper crust by the eastward expansion of the

magmatic arc during the Late Cretaceous (Haller et al., 2010; Aragón et al., 2013). This change in slab dip favored a strong increase in coupling of the subducting plates and the overriding plate (Horton and Fuentes, 2016). Growth strata in foreland basins have been detected in the continental Upper Cretaceous Chubut Group, Paso del Sapo Formations, and in the marine Paleocene Lefipán Formations (Gianni et al., 2015; Echaurren et al., 2016; Navarrete et al., 2016), which indicates that crustal shortening persisted throughout Late Cretaceous to Paleocene times (Echaurren et al., 2016; Horton, 2018). Subduction of mid-ocean ridges may have sustained this long-term and significant deformation, as the positive buoyancy of younger lithosphere tends to resist subduction (Cloos, 1993), and allowed the opening of a slab window during latest Cretaceous (Echaurren et al., 2016). A slab window model, supported by seismic tomography (Aragón et al., 2011), is generally accompanied by an isostatic uplift of the overriding plate and a dynamic topography related to limited deformation of the retroarc (Aragón et al., 2011, 2013; Ávila and Dávila, 2020).

Growth strata in the lower Eocene deposits are observed north and south of the area studied (Cobbold and Rossello, 2003; Charrier et al., 2007; Navarrete et al., 2016; Gianni et al., 2017), where only syn-extensional strata have been recognized in the upper Paleocene–Eocene Huitrera Formation associated with bimodal within-plate volcanism (Pilcaniyeu Belt; Fig. 3; Echaurren et al., 2016; Iannelli et al., 2018; Mazzoni et al., 1991). Cessation of the contraction between 40°S and 45°S during the Paleocene may be related to the resteeptening of the subducting slab induced by a sharp reduction in average trenchward velocity, an increase of slab pull forces after asthenospheric window development, and/or the decreasing buoyancy of oceanic segments (Suárez and De la Cruz, 2001; Aragón et al., 2011; Maloney et al., 2013; Echaurren et al., 2016; Horton, 2018). Pronounced slab rollback during the late Paleogene generated decoupling of the subducting plate and intake of hot atmosphere (De Ignacio et al., 2001; Encinas et al., 2016). The steepening of the slab is revealed by pervasive magmatism close to the Patagonian Precordillera (El Maitén Belt; Fig. 3; Iannelli et al., 2018; Paz et al., 2018; Rapela et al., 1988) and a modest extensional setting (Ventana Formation) reported in the whole Patagonia foreland (from Neuquén to Magallanes—Austral Basins; George et al., 2020; Horton et al., 2016; Orts et al., 2012). The Eocene–Miocene Somuncura Plateau and associated formations (e.g., El Buitre Formation) represented magmatism in the distal retroarc zone. Several origins have been proposed (e.g., slab detachment, plume-like

mantle upwelling) due to the complex geochemical signatures of these volcanic plateaus (De Ignacio et al., 2001; Kay et al., 2007; Aragón et al., 2013).

Trench-normal absolute velocity of the South American Plate remained low through ca. 23 Ma, when the break-up of the oceanic Farallon Plate into Nazca and Cocos Plate reorganized the plate convergence (Somoza, 1998; Lonsdale, 2005). This new configuration allowed an increase of interplate coupling that was not necessarily linked to a change of slab dip (Cerpa et al., 2018; Schellart, 2020). Resumption of the upper plate shortening is recorded along the Patagonian Precordillera and associated with the Miocene rejuvenation of the North Patagonian Batholith (Echaurren et al., 2016). Mild contractional deformation of the foreland has been proposed based on the growth strata documented in the early–middle Miocene foreland basins known as the Ñirihuau and Collón Curá Basins (Fig. 2; Echaurren et al., 2016; Orts et al., 2012; Ramos et al., 2011). Substantial Miocene deformation controlled by former heterogeneities is also suggested in the foreland (Bilmes et al., 2013; Gianni et al., 2015).

MATERIALS AND METHODS

The low closure temperatures of apatite (U–Th)/He (AHe, ~65 °C; e.g., Flowers et al., 2009; Gautheron et al., 2009) and apatite fission track (AFT, ~110 °C; e.g., Ketcham et al., 2007) systems provide information on cooling histories and exhumation within the upper crust. In this study, we present 33 AHe and 31 new AFT ages from samples collected from the Patagonian Precordillera and its broken foreland between 40°S and 45°S. Fifteen of the new AFT ages (with track measurements) were obtained from the same samples that further yielded 34 single-grain AHe ages published by Savignano et al. (2016), and thus an extensive data set was achieved (Fig. 2). Geographic coordinates, elevation, formation (mainly metamorphic basement, Jurassic sedimentary rocks, and Cretaceous granitoids), stratigraphic age, and rock lithology of all samples are included in Table 1.

Apatite Fission Tracks (AFT)

We performed AFT analysis at the University of Padua, Italy. Apatite grains were mounted in epoxy resin, polished, and etched at 5.5 M HNO₃ for 20 sec at 20 °C to reveal spontaneous tracks. The samples were analyzed by applying the external detector method (Gleadow, 1981) using low-uranium muscovite foils as an external detector to cover apatite mounts and then irradiated at the Radiation Center of Oregon State

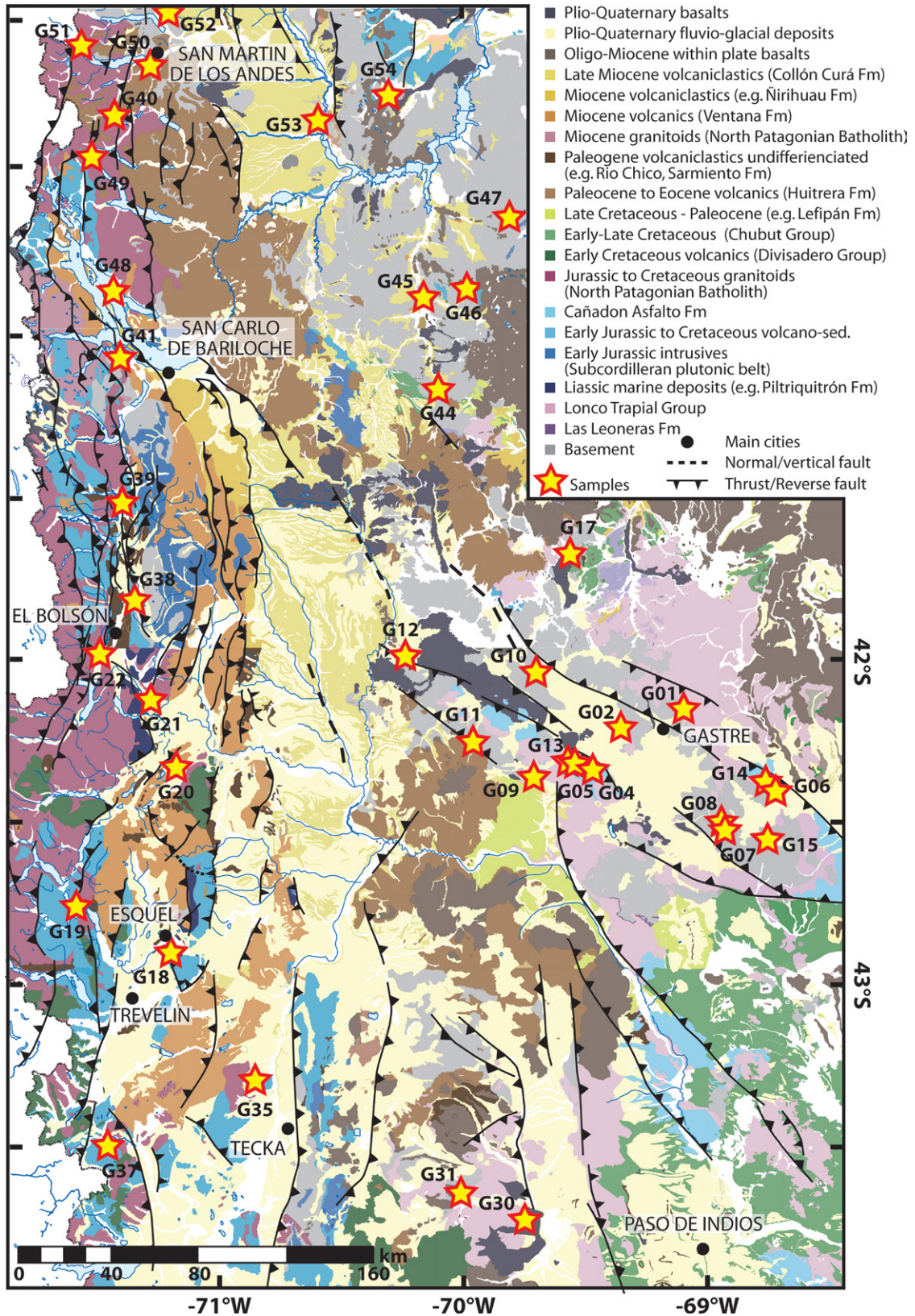


Figure 3. Geological map of the study area shows the locations of samples used in this study (modified after Anselmi et al., 2004; Ardolino et al., 2011; Cucchi et al., 2001, 1998; Escosteguy et al., 2013; Giacosa et al., 2001; González et al., 2000; Haller et al., 2010; Lizuáin et al., 2010; Lizuáin and Nieto, 2011; Orts et al., 2015; Remesal et al., 2001; Savignano et al., 2016; Silva Nieto et al., 2005).

TABLE 1. SUMMARY OF SAMPLE INFORMATION AND APATITE FISSION TRACK (AFT) DATA

Samples ¹	Field*		Elev. (m)	Lithology	Formation	Stratigraphic age	AFT ages						AFT length						
	Latitude (°S)	Longitude (°W)					AFT (Ma)	σ	Ns	μ S	Ni	ρ i	Nd	ρ D	$P(\chi^2)$	MTL (μ m)	σ	n°	Dpar
G01	-42.1928	-69.1656	1134	granite	Lipetren	Triassic	96.3	6.4	400	5.90	922	12.12	4798	11.56	93.29	12.86	0.18	80	1.88
G02	-42.2658	-69.4086	929	granite	Mamil Choique	Permian	68	5.2	268	5.15	775	14.89	4798	11.46	99.68	11.95	0.23	66	1.81
G04	-42.3878	-69.5219	997	granite	Mamil Choique	Permian	87.3	4.3	867	10.86	1938	24.27	4798	11.39	98.3				
G05	-42.3694	-69.6292	963	conglomerate	Cañadon Asfalto	Upper Jurassic	108.2	11.2	155	4.15	282	7.55	8875	11.51	96.7				
G06	-42.4444	-68.7803	1150	arkose	Cañadon Asfalto	Upper Jurassic	109.2	7.8	352	3.23	625	5.73	8875	11.34	100				
G07	-42.5597	-69.0039	1070	granite	Mamil Choique	Lower Permian	154.4	6	2211	39.86	2832	51.05	4798	11.6	99.9	12.47	0.13	100	1.88
G08	-42.5639	-69.0042	1043	granite	Mamil Choique	Lower Permian	74.1	4	643	12.01	1670	31.20	4798	11.22	73.5	12.11	0.23	92	2.33
G09	-42.4131	-69.7822	995	arkose	Cañadon Asfalto	Upper Jurassic	99.9	5.6	602	5.81	1152	11.11	8875	11.17	91	12.02	0.27	56	2.39
G10	-42.0953	-69.7749	1060	granite	Mamil Choique	Lower Permian													
G11	-42.3114	-70.0367	999	dyke (granite)	Mamil Choique	Lower Permian													
G12	-42.0353	-70.2992	976	granite	Mamil Choique	Lower Permian	112	6	710	11.24	1192	18.87	8875	11	88.66				
G13	-42.3736	-69.6039	973	sandstone	Mamil Choique	Upper Jurassic	95	4.8	1475	15.71	2904	30.93	8875	10.94	63	11.73	0.19	61	1.90
G14	-42.4253	-68.8347	1177	sandstone	Cañadon Asfalto	Upper Jurassic	112.6	8.6	1184	13.84	2001	23.40	8875	10.89	92.78				
G15	-42.5861	-68.8128	1103	granite	Mamil Choique	Lower Permian	87.1	9	147	3.19	313	6.80	4798	10.83	99				
G17	-41.7119	-69.6192	1275	granite	Mamil Choique	Lower Permian	73.6	3.7	718	13.20	1794	32.99	8875	10.72	99.55	12.70	0.16	94	1.67
G18	-42.9306	-71.2606	617	granite	Subcordilleran	Lower Jurassic													
G19	-42.8064	-71.6608	576	granite	Plutonic Belt Patagonian Batholith	Upper Cretaceous													
G20	-42.3847	-71.2453	663	granite	Leleque	Upper Jurassic													
G21	-42.1672	-71.3572	616	granodiorite	Subcordilleran	Lower Jurassic	11.5	1.3	92	2.08	1464	33.06	4798	10.6	100				
G22	-42.0303	-71.5761	275	granite	Plutonic Belt Patagonian Batholith	Upper Cretaceous	14.8	1.3	162	3.14	1995	38.47	8875	10.55	36.74				
G30	-43.7439	-69.8186	670	sandstone	Osta Arena	Lower Jurassic	89.8	8.3	211	2.11	416	4.15	5000	10.3	100	12.61	0.15	65	1.39
G31	-43.6650	-70.0839	825	sandstone	Tepuel Group	Carboniferous to Permian	67.4	4.6	418	9.98	1078	25.74	5000	10.1	98.9				
G35	-43.3244	-70.8961	875	granitoid	Rio Hielo	Cretaceous	73.5	10.4	76	1.98	178	4.64	5000	10	99.98	12.14	0.2	25	1.33
G37	-43.5250	-71.5181	473	granitoid	Rio Hielo	Cretaceous													
G38	-41.8508	-71.4219	627	granodiorite	Complejo Colohuincul	Lower Permian	8.6	1	88	1.34	1743	26.57	5000	9.85	100				
G39	-41.5564	-71.4806	731	granite	Patagonian Batholith	Lower Cretaceous													
G40	-40.3447	-71.5064	898	granodiorite	Complejo Colohuincul	Lower Permian	14.2	1.7	86	1.14	1026	13.61	5000	9.77	99.95	13.87	0.09	60	1.34
G41	-41.1061	-71.4831	849	granite	Patagonian Batholith	Lower Cretaceous	9	1.1	73	2.03	1364	37.95	5000	9.69	99.37				
G44	-41.2089	-70.1667	999	granite	Plutonitas	Lower Jurassic	83.5	5.6	489	4.84	968	9.58	5000	9.61	94.66	12.09	0.1	61	1.32
G45	-40.9181	-70.2247	810	granodiorite	Pilcaniyeu	Lower Permian	77.9	5.7	368	6.74	775	14.20	5000	9.54	97.69				
G46	-40.9017	-70.0461	1189	granodiorite	Mamil Choique	Lower Permian	71.6	5.1	382	5.76	869	13.10	5000	9.46	81.3				
G47	-40.6692	-69.8833	1298	granodiorite	Mamil Choique	Lower Permian	81.8	4.9	683	10.54	1349	20.81	5000	9.39	88.24	11.90	0.15	33	1.33
G48	-40.8936	-71.4950	805	granodiorite	Los Machis	Up. Jurassic to Cretaceous	14.5	1.2	188	2.79	2093	31.03	5000	9.31	99.85				
G49	-40.4853	-71.5894	903	granodiorite	Los Machis	Up. Jurassic to Cretaceous	6.9	0.9	60	1.07	1387	24.84	5000	9.23	100				
G50	-40.1956	-71.3614	976	granodiorite	Complejo Colohuincul	Lower Permian	4.9	0.6	66	1.12	2131	36.27	5000	9.15	100				
G51	-40.1289	-71.6456	791	tonalite	Los Machis	Up. Jurassic to Cretaceous	8.1	1.1	65	0.92	1242	17.56	5000	9	99.34				
G53	-40.3683	-70.6619	645	granite	Cushamen	Devonian to Carboniferous	59.3	4.2	392	6.66	1015	17.24	5000	8.92	99.98	12.66	0.11	86	1.29
G54	-40.2822	-70.3803	986	granodiorite	Mamil Choique	Lower Permian	69.6	4.6	486	8.69	1063	19.00	5000	8.85	100	12.83	0.13	100	1.28

Notes: Central ages reported with a confidence interval of $\pm 1\sigma$. N—number of apatite crystal counted; and ρ —track density ($\times 10^5$ tracks/cm²); subscripts s, l, and d denote spontaneous, induced, and dosimeter, respectively; $P(\chi^2)$ —probability of obtaining a Chi-square value for n degrees of freedom; Dpair—mean diameter of fission-track etch pit parallel to the c-axis. MTL—Mean Track Length.

*Longitude and latitude coordinates are given in WGS84.

¹Zeta = 345 ± 8 .

²Zeta = 346 ± 12 .

University with a nominal fluence of 9×10^{15} neutrons/cm². After irradiation, we etched mica detectors for 40 min in 40% HF at 20 °C to reveal induced tracks. We counted tracks and measured track length distribution using an Olympus optical microscope at a magnification of $\times 1250$. We carried out age calculations and statistics with Trackkey software (Dunkl, 2002). We report AFT ages as central age with 1σ errors (Galbraith and Laslett, 1993) using a zeta calibration approach (Hurford and Green, 1983) with a zeta value of 345 ± 8 (samples G1-G22) and a zeta value of 346 ± 12 (samples G30-G55) for the CN5 dosimeter glass. Dpar measurements were used to characterize the chemical kinetic properties of the apatite crystals (Burtner et al., 1994). Both track density ratio and average track etch pit diameter (Dpar) were recorded for 20 grains per sample. The results are presented in Table 1.

Apatite (U-Th-Sm)/He (AHe)

The first steps of AHe dating involved apatite picking at the University of Paris-Saclay, Orsay, France. Apatite grains were selected carefully according to their morphology, size (minimum width of 60 μ m), and lack of visible inclusions or grain boundary phases (Murray et al., 2014) and then placed into a Niobium basket for He extraction. From one to three grains were dated per sample, depending on sample apatite quality. The Niobium baskets were heated twice using a diode laser at 1030 ± 50 °C for 5 min, allowing for total He degassing and to check the presence of He trapped in small inclusions (Fillon et al., 2013). The ⁴He content was determined by comparison with a known amount of ³He spike added during analysis. After He extraction, Nb baskets were placed into single-use polypropylene vials. Apatite grains were dissolved for 3 h at 70 °C in a 50 μ L HNO₃ 5N⁻ solution containing a known content of ²³⁵U, ²³⁰Th, and ¹⁴⁹Sm, and additional 50 μ L HNO₃ 5N⁻ and then filled with 0.9 mL of ultrapure MQ water. The final solution was measured for U, Th, and Sm concentrations by quadrupole inductively coupled plasma (ICP-quadrupole) mass spectrometry (collision cell technology [CCT] Thermo-Electron at LSCE, Gif/Yvette, France). The analysis was calibrated using external age standards, including Limberg Tuff and Durango apatites. Mean AHe ages of 16.0 ± 1.4 Ma and 31.1 ± 2.1 Ma have been measured for the Limberg Tuff and yellow Durango apatite, respectively, which agree with published data (i.e., 16.8 ± 1.1 Ma and 31.0 ± 1.0 Ma; Kraml et al., 2006; McDowell et al., 2005). Single ages were corrected using the calculated ejection factor FT, determined using the Monte Carlo simulation technique of Ketcham et al. (2011); the equivalent-sphere

radius was calculated using the procedure of Gautheron and Tassan-Got (2010). Single-grain apatite He ages and supporting data are presented in Table 2. The 1σ error for single-grain AHe ages should be considered as 9%, reflecting the sum of errors in the ejection-factor correction and age dispersion of the standards.

Time–Temperature Modeling

In this work we used the QTQt software (version PC 5.7.0) to model 30 samples, including those never before modeled, from Savignano et al. (2016). The program allows inversion of the AFT annealing and AHe diffusion parameters with the Markov chain Monte Carlo method (Gallagher et al., 2009; Gallagher, 2012). The inversion code incorporates kinetic models of He diffusion in apatite (Flowers et al., 2009; Gautheron et al., 2009) and AFT annealing in the multi-kinetic model (Ketcham et al., 2007). The modeling procedure is detailed in Gallagher (2012). The input parameters used to model each profile are: (1) central AFT ages, (2) track length distribution, (3) Dpar values, and (4) single-grain AHe ages with grain size and chemical characteristics. Chemical composition ranges of the apatites analyzed were taken into consideration during both AFT and AHe modeling by imposing the mean measured Dpar values for the sample following Gautheron et al. (2013). Thermal history constraints included: (1) age and emplacement depth of intrusive bodies such as the Permian Mamil Choique Formation ($t = 275 \pm 25$ Ma, $T = 350 \pm 50$ °C), the Lower Jurassic Subcordilleran Batholith and equivalents ($t = 190 \pm 20$ Ma, $T = 350 \pm 50$ °C), the Upper Jurassic to Lower Cretaceous North Patagonian Batholith ($t = 135 \pm 35$ Ma, $T = 350 \pm 50$ °C), and Upper Cretaceous shallow intrusions ($t = 80 \pm 20$ Ma and $T = 100 \pm 20$ °C); (2) depositional age of sedimentary rocks such as the Osta Arena Formation (Lower Jurassic) and Cañadon Asfalto Formation (Upper Jurassic); (3) age of the unconformity (Lower Jurassic) on top of the basement; and (4) present day temperature (10 ± 10 °C for all of the rocks). Thermal history simulation results were obtained taking into account the influence of α -recoil damage, grain size, and apatite kinetic properties.

RESULTS

A homogeneous single grain AFT population (χ^2 test passed) was detected in all of the samples, whereas significant intra-sample variability was observed in only two cases among the AHe data despite the large variety of rock types and U-Th-Sm composition (in both these latter samples, apatites derive from Paleozoic rocks from

the foreland). No particular relationships occur between age, eU ($eU = [U] + 0.235[Th] + 0.047[Sm]$), and grain radius. AFT ages obtained are in all instances older than AHe ages, as is expected given the closure temperatures. The regional picture is characterized by a marked thermochronological age difference between the Patagonian Precordillera and the broken foreland (Figs. 1, 2, and 4). In fact, the samples from the Precordillera show consistent middle Miocene to Pliocene cooling ages. In contrast, AFT and AHe ages in the broken foreland range from 154.4 ± 6.0 Ma to 59.3 ± 4.2 Ma, and from 109.2 ± 9.8 Ma to 26.9 ± 2.4 Ma, respectively. Both AFT and AHe ages are always younger than the depositional ages of the sedimentary rocks sampled. This testifies that all samples were affected by a significant heating that almost completely reset both the AFT and AHe systems. It is noteworthy that the samples from the broken foreland display short fission track lengths (Table 1), thus suggesting a long residence in the so-called Partial Annealing Zone (~ 60 – 120 °C, Green et al., 1989). Cretaceous granitoids collected in the Patagonian Precordillera record Late Neogene AFT and AHe cooling ages with the exception of three samples characterized by older AFT and/or AHe ages (Fig. 1).

Paleotemperatures were extracted from the best-fit models (Fig. 4; Figs. S1A and S1B¹) at different times and then plotted on the map of Figure 5. During Early Jurassic times, most of the samples were at shallow depths (at temperatures between 40 °C and 80 °C), whereas some granitoids were emplaced along the so-called Subcordillera Plutonic Belt (red dots in Fig. 5A). Between the Early and early Late Cretaceous, maximum burial temperatures exceeding or very close to the total reset limit for fission tracks in apatite (i.e., ~ 120 °C; Green et al., 1989) were reached all across the foreland. Soon after, exhumation of the foreland samples started at very slow rates. From the Late Cretaceous, a clear differentiation occurred between the foreland and the orogen. Samples from the latter still lay at greater depth (except for a few intrusions away from the basins and therefore not affected by any burial, which were already close to the surface). The foreland area remained quite stable for the following 70 m.y., whereas the Patagonian Precordillera was affected by rapid cooling during late Miocene–Pliocene times.

¹Supplemental Material. Input files for inverse thermal modeling of the results presented in Figures S1a and S1b. Please visit <https://doi.org/10.1130/GSAB.S.13863536> to access the supplemental material, and contact editing@geosociety.org with any questions.

TABLE 2. APATITE (U-Th)/HE SINGLE GRAIN DATA

Samples	Latitude (°S)	Longitude (°W)	Elev. (m)	Weight (μ g)	Rs (μ m)	FT	⁴ He (ncc/g)	U (ppm)	Th (ppm)	Sm (ppm)	Th/U	eU (ppm)	AHe age (Ma)	Corrected age (Ma)	Error (Ma)
<i>Data from Savignano et al. (2016)</i>															
G01B	-42.1928	-69.1656	1134.00	1.70	38.00	0.64	481259.60	91	31	151	0.30	98	40.00	62.10	5.60
G02B	-42.2658	-69.4086	929.00	1.80	41.00	0.72	159254.40	18	59	82	3.30	32	40.60	56.50	5.10
G02C	-42.2658	-69.4086	929.00	0.90	35.00	0.66	70897.90	9	20	486	2.20	14	33.00	49.90	4.50
G04A	-42.3878	-69.5219	997.00	3.80	53.00	0.79	204917.20	21	22	66	1.00	27	62.70	79.90	7.20
G04B	-42.3878	-69.5219	997.00	1.40	41.00	0.71	257276.90	32	33	97	1.00	40	51.90	73.60	6.60
G04C	-42.3878	-69.5219	997.00	1.60	44.00	0.68	729467.20	83	96	17	1.20	105	57.30	83.80	7.50
G05C	-42.3694	-69.6292	963.00	1.80	46.00	0.75	116142.70	43	20	65	0.50	47	20.10	26.90	2.40
G06C	-42.4444	-68.7803	1150.00	3.50	55.00	0.78	70495.90	22	19	66	0.90	27	21.60	27.70	2.50
G07A	-42.5597	-69.0039	1070.00	2.60	52.00	0.73	1256944.80	134	3	152	0.00	135	76.50	104.60	9.40
G07C	-42.5597	-69.0039	1070.00	3.40	55.00	0.75	1587006.90	159	9	66	0.10	161	81.40	109.20	9.80
G08A	-42.5639	-69.0042	1043.00	1.90	39.00	0.69	113056.00	15	8	133	0.50	17	51.40	74.50	6.70
G09A	-42.4131	-69.7822	995.00	0.50	32.00	0.57	260075.30	33	89	933	2.70	54	35.10	61.40	5.50
G09B	-42.4131	-69.7822	995.00	0.90	33.00	0.63	124150.00	19	50	141	2.70	31	32.30	51.60	4.60
G09C	-42.4131	-69.7822	995.00	1.60	43.00	0.68	149903.50	19	67	58	3.40	36	34.60	51.10	4.60
G10B	-42.0953	69.7749	1060.00	8.80	77.00	0.85	172830.10	17	6	29	0.30	19	75.10	88.70	8.00
G10C	-42.0953	69.7749	1060.00	4.50	60.00	0.79	163455.50	18	7	83	0.40	19	67.60	85.20	7.70
G11B	-42.3114	-70.0367	999.00	1.30	38.00	0.69	89896.40	17	22	98	1.20	23	31.80	46.40	4.20
G11C	-42.3114	-70.0367	999.00	1.60	43.00	0.72	40621.00	8	3	114	0.40	9	34.10	47.50	4.30
G12A	-42.0353	-70.2992	976.00	3.90	53.00	0.78	170929.50	15	17	104	1.10	19	71.40	91.20	8.20
G12B	-42.0353	-70.2992	976.00	3.30	52.00	0.76	348509.60	50	13	159	0.30	53	53.30	70.20	6.30
G13B	-42.3736	-69.6039	973.00	3.90	58.00	0.80	239706.70	27	40	51	1.50	37	53.30	66.80	6.00
G13C	-42.3736	-69.6039	973.00	7.00	70.00	0.82	28134.20	3	15	79	4.40	7	30.00	36.40	3.30
G14A	-42.4253	-68.8347	1177.00	3.90	58.00	0.79	291854.30	35	83	61	2.40	56	43.30	55.00	4.90
G14C	-42.4253	-68.8347	1177.00	4.10	54.00	0.77	357806.40	64	74	89	1.20	82	36.10	46.90	4.20
G15B	-42.5861	-68.8128	1103.00	4.10	41.00	0.77	26296.80	3	11	52	4.30	5	39.20	51.00	4.60
G15C	-42.5861	-68.8128	1103.00	1.60	45.00	0.69	65107.30	5	23	135	4.30	11	44.90	65.40	5.90
G17C	-41.7119	-69.6192	1275.00	1.10	35.00	0.65	206061.00	25	13	126	0.50	28	58.10	88.90	8.00
G18B	-42.9306	-71.2606	617.00	2.50	47.00	0.73	42608.50	103	83	208	0.80	123	2.80	3.90	0.40
G19B	-42.8064	-71.6608	576.00	1.80	42.00	0.71	200378.00	26	95	249	3.60	49	3.30	4.60	0.40
G19C	-42.8064	-71.6608	576.00	1.30	39.00	0.69	11635.10	53	61	236	1.10	68	1.40	2.00	0.20
G20A	-42.3847	-71.2453	663.00	1.50	42.00	0.67	20451.30	11	50	164	4.70	23	7.20	10.60	1.00
G20B	-42.3847	-71.2453	663.00	0.90	36.00	0.68	12081.70	13	33	140	2.50	21	4.50	6.70	0.60
G20C	-42.3847	-71.2453	663.00	3.30	51.00	0.73	5681.20	6	24	85	3.80	12	3.70	5.00	0.50
G21A	-42.1672	-71.3572	616.00	0.90	20.00	0.61	41763.50	51	25	152	0.50	57	5.90	9.80	0.90
G21B	-42.1672	-71.3572	616.00	1.10	37.00	0.64	32364.80	38	30	237	0.80	45	5.80	9.10	0.80
G21C	-42.1672	-71.3572	616.00	1.90	44.00	0.73	16467.80	23	14	79	0.60	26	5.10	7.00	0.60
G22B	-42.0303	-71.5761	275.00	1.50	45.00	0.69	33055.70	84	185	70	2.20	129	2.10	3.10	0.30
G22C	-42.0303	-71.5761	275.00	2.00	46.00	0.73	19459.80	45	109	127	2.40	71	2.20	3.10	0.30
<i>New data</i>															
G30A	-43.7439	-69.8186	670.00	12.37	78.30	0.85	126233.00	4	39	76	9.10	14	73.40	85.90	0.70
G30B	-43.7439	-69.8186	670.00	3.58	55.60	0.78	145207.00	6	48	209	8.20	18	63.00	80.70	0.60
G30C	-43.7439	-69.8186	670.00	8.72	71.60	0.82	178090.00	6	50	107	9.20	18	81.20	98.80	0.80
G31A	-43.6650	-70.0839	825.00	5.46	59.00	0.79	0.00	8	21	131	2.50	14	52.30	66.40	5.30
G31C	-43.6650	-70.0839	825.00	2.95	43.20	0.68	0.00	11	45	102	4.30	21	45.20	66.40	5.30
G31D	-43.6650	-70.0839	825.00	5.25	56.40	0.75	0.00	5	32	91	6.40	13	41.40	55.20	4.40
G35A	-43.3244	-70.8961	875.00	4.23	46.70	0.72	22167.00	5	18	80	3.40	10	17.50	24.30	1.90
G35B	-43.3244	-70.8961	875.00	5.64	52.40	0.75	14432.00	4	14	51	3.20	8	15.10	20.10	1.60
G37A	-43.5250	-71.5181	473.00	0.54	27.80	0.56	141653.00	6	44	422	8.00	16	60.00	106.80	8.50
G37B	-43.5250	-71.5181	473.00	0.67	28.30	0.60	149258.00	9	31	343	3.50	17	64.40	107.80	8.60
G38A	-41.8508	-71.4219	627.00	1.62	37.40	0.68	27338.00	30	31	90	1.00	37	6.00	8.80	0.70
G38B	-41.8508	-71.4219	627.00	1.65	39.40	0.68	35968.00	35	49	92	1.40	46	6.40	9.40	0.80
G38C	-41.8508	-71.4219	627.00	2.77	50.50	0.72	16316.00	25	39	93	1.60	34	3.90	5.40	0.40
G39A	-41.5564	-71.4806	731.00	0.76	30.30	0.59	39981.00	6	12	242	2.10	9	31.60	53.70	0.30
G39B	-41.5564	-71.4806	731.00	0.76	26.20	0.59	35918.00	6	17	303	2.90	10	23.80	40.50	0.20
G39C	-41.5564	-71.4806	731.00	0.36	25.00	0.53	115956.00	15	31	601	2.00	23	35.30	66.20	0.40
G40A	-40.3447	-71.5064	898.00	0.92	33.70	0.64	13772.00	22	59	55	2.70	36	3.20	5.00	0.40
G40B	-40.3447	-71.5064	898.00	0.60	29.80	0.60	32916.00	23	62	95	2.60	38	7.00	11.80	0.90
G41A	-41.1061	-71.4831	849.00	0.85	31.40	0.65	103534.00	60	43	177	0.70	70	12.00	18.50	0.10
G41B	-41.1061	-71.4831	849.00	2.80	48.70	0.78	139480.00	52	47	143	0.90	63	18.00	23.20	0.20
G41C	-41.1061	-71.4831	849.00	0.60	28.60	0.57	133871.00	94	68	226	0.70	110	9.90	17.30	0.10
G44B	-41.2089	-70.1667	999.00	2.26	44.80	0.69	63247.00	9	1	95	0.10	9	53.10	77.10	6.20
G44C	-41.2089	-70.1667	999.00	3.63	50.40	0.72	303657.00	35	41	123	1.20	45	55.40	76.70	6.10
G48A	-40.8936	-71.4950	805.00	1.79	42.80	0.68	22054.00	34	57	177	1.70	48	3.70	5.50	0.40
G48B	-40.8936	-71.4950	805.00	2.91	50.30	0.75	23517.00	31	51	136	1.60	44	4.40	5.80	0.50
G48C	-40.8936	-71.4950	805.00	2.48	46.50	0.73	18720.00	19	38	130	1.90	28	5.30	7.30	0.60
G49A	-40.4853	-71.5894	903.00	0.74	32.90	0.59	37522.00	35	55	143	1.60	49	6.30	10.70	0.90
G49B	-40.4853	-71.5894	903.00	1.60	39.00	0.65	23932.00	23	58	134	2.60	37	5.30	8.20	0.70
G50A	-40.1956	-71.3614	976.00	0.93	32.60	0.62	23618.00	73	9	245	0.10	75	2.50	4.10	0.30
G50B	-40.1956	-71.3614	976.00	2.48	48.90	0.72	18111.00	44	7	145	0.10	45	3.20	4.50	0.40
G50C	-40.1956	-71.3614	976.00	1.41	41.00	0.66	45107.00	106	31	284	0.30	114	3.20	4.80	0.40
G51A	-40.1289	-71.6456	791.00	2.26	45.90	0.73	6474.00	15	19	58	1.20	20	2.70	3.60	0.00
G51B	-40.1289	-71.6456	791.00	3.73	53.00	0.76	2563.00	10	13	37	1.30	13	1.60	2.10	0.00

Notes: Rs—sphere equivalent radius of hexagonal crystal with the same surface/volume ratio; FT—geometric correction factor for age calculation; eU—effective uranium concentration.

DISCUSSION

Best-fit thermal histories derived from the inverse modeling of samples collected in the foreland show maximum burial conditions at temperatures higher than 110 °C (Figs. 5 and

6A). The present-day average geothermal gradient is estimated at 34 ± 11 °C/km for the upper crust in the north Patagonian Cordillera based on regional surface heat flow measurements and thermal conductivities for granitoids (Hamza and Muñoz, 1996; Seipold, 1998; Muñoz, 1999;

Thomson, 2002; Adriasola et al., 2006; Sachse et al., 2016). Nevertheless, the geothermal gradient in the north Patagonian Precordillera and its foreland may have changed over time, especially due to magmatic events, slab window opening, or crustal thinning. Although the magmatic arc

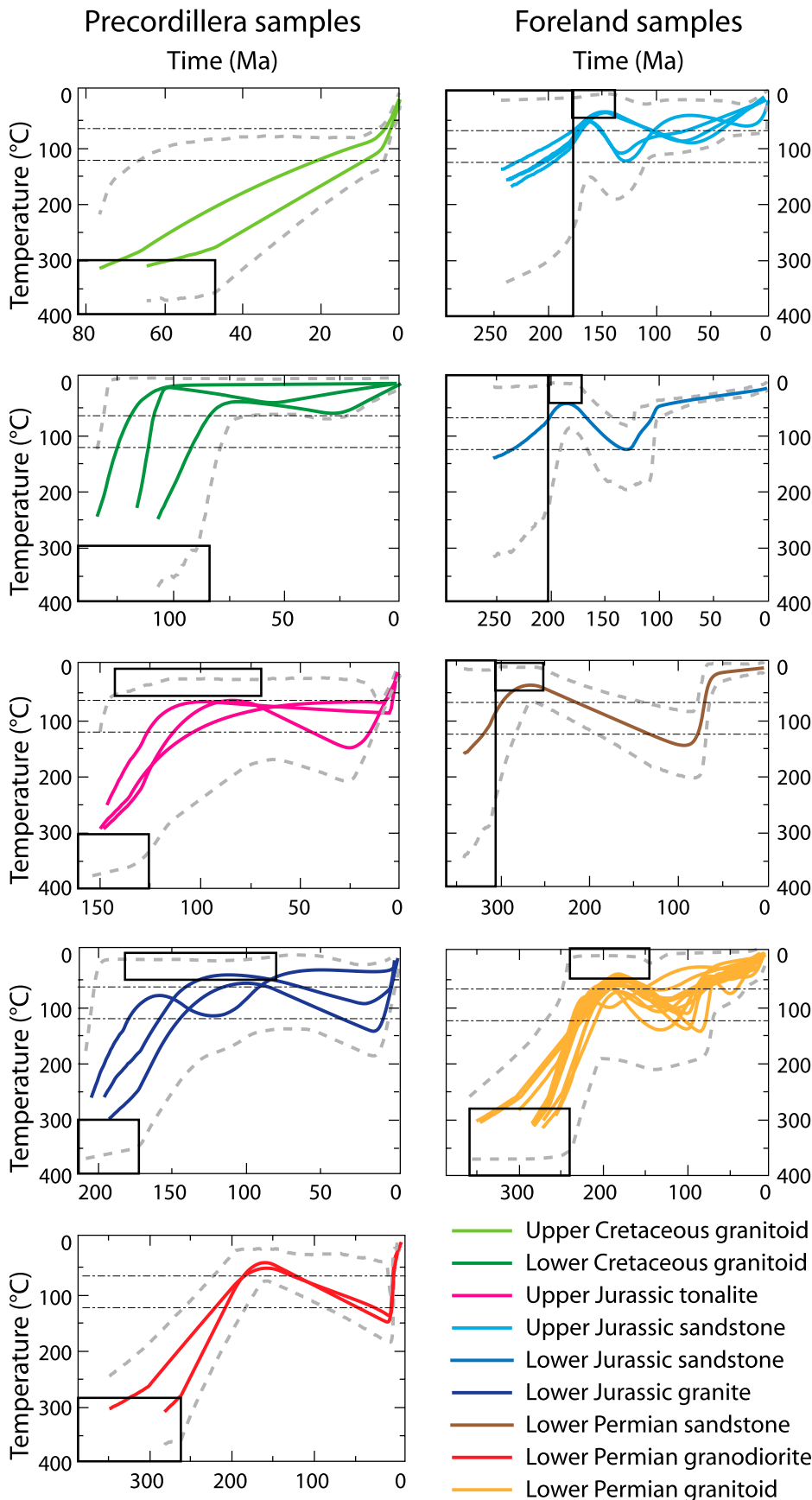


Figure 4. Time–temperature history from QTQt for all samples subdivided according to their locations (Patagonian Precordillera or broken foreland, left and right columns, respectively), age, and lithology are shown. Colored solid lines show the best-fit, time–temperature model of each sample (each diagram includes samples with similar age and lithology). Gray dotted lines show 95% confidence intervals for each group of samples. Boxes show initial constraints: deposition time for sedimentary samples, high-temperature box for emplacement age of intrusive rocks, and age of the unconformity between the top of the basement and overlying formations. Thin dotted lines show boundaries of the Partial Annealing Zone.

migrated through time either toward the eastern foreland or the trench (Fig. 2), thermal modeling does not show any particular thermal event that could be potentially related to the shifts of the magmatic arc. However, within the general framework of progressive cooling since the Late Cretaceous, a significant change in the near-surface geothermal gradient—perhaps at a local scale—cannot be completely ruled out. Thus, given that a precise estimation of paleo-geothermal gradients is not possible, we can only roughly estimate a regional burial of 3–4 km across the foreland, assuming variations around an average geothermal gradient of ~ 30 °C/km. Such a burial may be easily explained by the thickness of the Jurassic–Lower Cretaceous sedimentary succession deposited in the half-graben systems forming the Cañadón Asfalto Rift Basin (Zafarana and Somoza, 2012; Figari et al., 2015). Significantly higher values of burial, which are not easily explainable by sediment thickness alone, are not likely as they would imply lower geothermal gradients, which is actually not consistent with the Jurassic–Early Cretaceous back-arc setting. The samples from the Patagonian Precordillera were collected close to the thick successions deposited in the Piltriquitrón and Rio Mayo Basins (Cesari, 1977; Ghorzi, 1979) for which basin subsidence was related to back-arc extension triggered by ongoing slab roll-back and slab steepening (Fig. 6B; Horton, 2018). Also, for these samples, an exhumation of 2.5–4 km may be envisaged.

Regional exhumation recorded by our data is consistent with the unconformity recognized between the Jurassic–Lower Cretaceous succession and the synorogenic Upper Cretaceous deposits (Gianni et al., 2015). This regional exhumation was favored by the strong increase in coupling of the subducting plates and the overriding plate

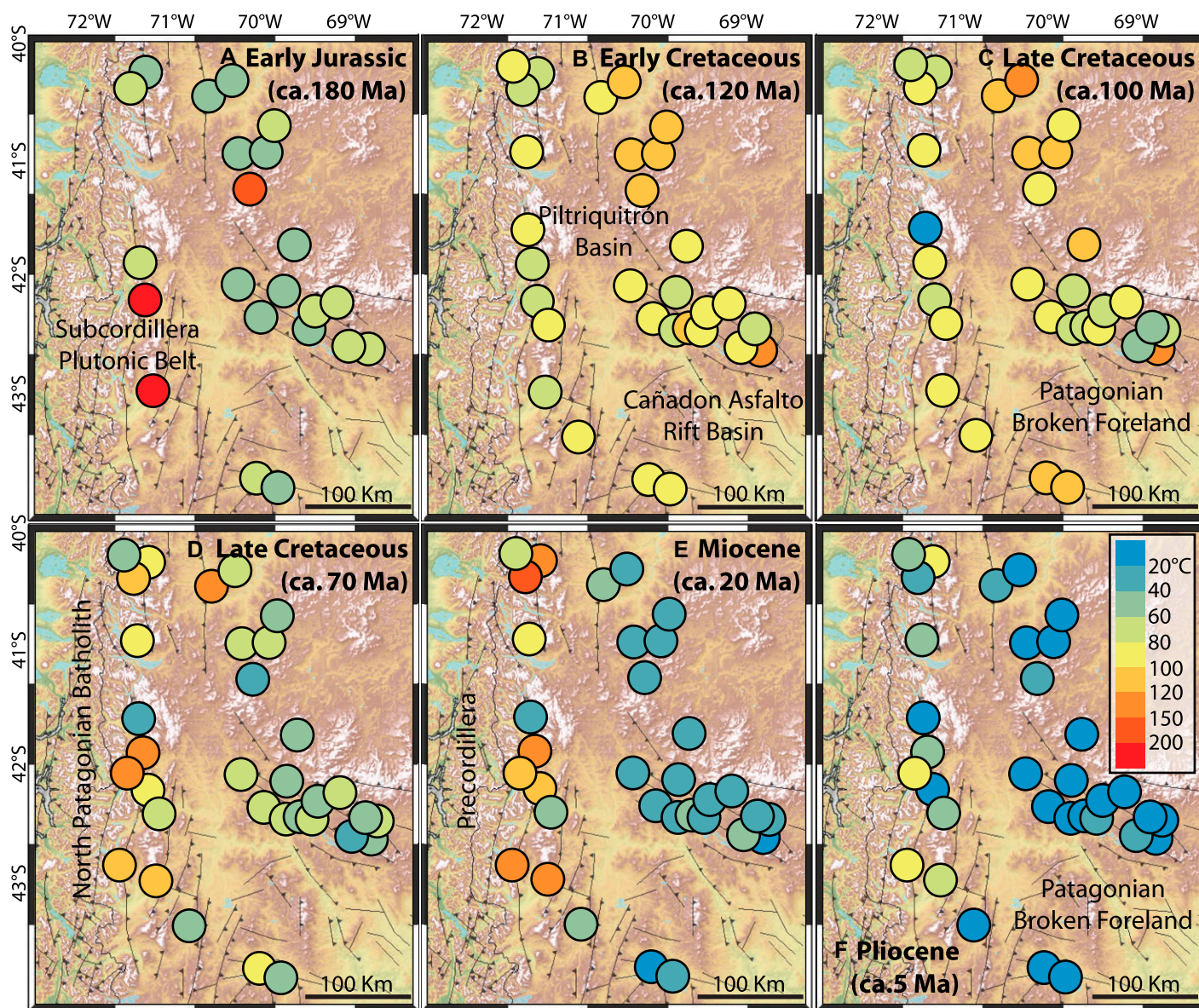


Figure 5. (A–F) Reconstructed Early Jurassic to Pliocene paleotemperature evolution for the samples collected in northern Patagonia is shown. These diagrams indicate a similar thermal history for the Patagonian Precordillera and the broken foreland during most of the Mesozoic. The samples from the broken foreland reached low temperatures, and therefore near-surface conditions, during the Late Cretaceous. A differentiation between these areas persisted throughout the Cenozoic.

(Horton and Fuentes, 2016), which also resulted in regional uplift (Fig. 6C; e.g., Mescua et al., 2013). Strong coupling is related to slab shallowing induced by the change of absolute motion of the South American Plate, which became west directed (Maloney et al., 2013). Overriding plate kinematics exert a first-order control on slab dip evolution (Cerpa et al., 2018). This is dominant over oceanic subducting plate convergence as demonstrated in the Central Andes, where an increase in deformation occurred during stages of convergence rate decrease (Oncken et al., 2006). Slab shallowing is recognized to produce

significant foreland uplift, as is observed along the present day flat-slab in central Chile (Ramos et al., 2002) and Peru (Bishop et al., 2018). Examples in the geological record include the Late Cretaceous to early Eocene, low-angle subduction in the Laramide orogen, USA (Jordán et al., 1983; Fan and Carrapa, 2014) and Paleocene low-angle subduction in Alaska, USA (Finzel et al., 2011). In northern Patagonia, exhumation of the overriding plate during the Late Cretaceous may have been further enhanced by the subduction of mid-ocean ridges, further triggering shallow subduction and possibly also open-

ing of a slab window (Aragón et al., 2011). This latter may have added a further component of foreland uplift (Ávila and Dávila, 2020; Guillaume et al., 2009; Fig. 6D). The integrated uplift and coeval erosion may account for the cooling ages recorded over the whole northern Patagonia region and particularly in the broken foreland. Although a significant spread of cooling ages characterizes the foreland samples (Fig. 2), almost all of them record exhumation during upper plate shortening, around the Late Cretaceous deformation peak and through the early Paleocene (Fig. 6D). Actually, few single grain ages from

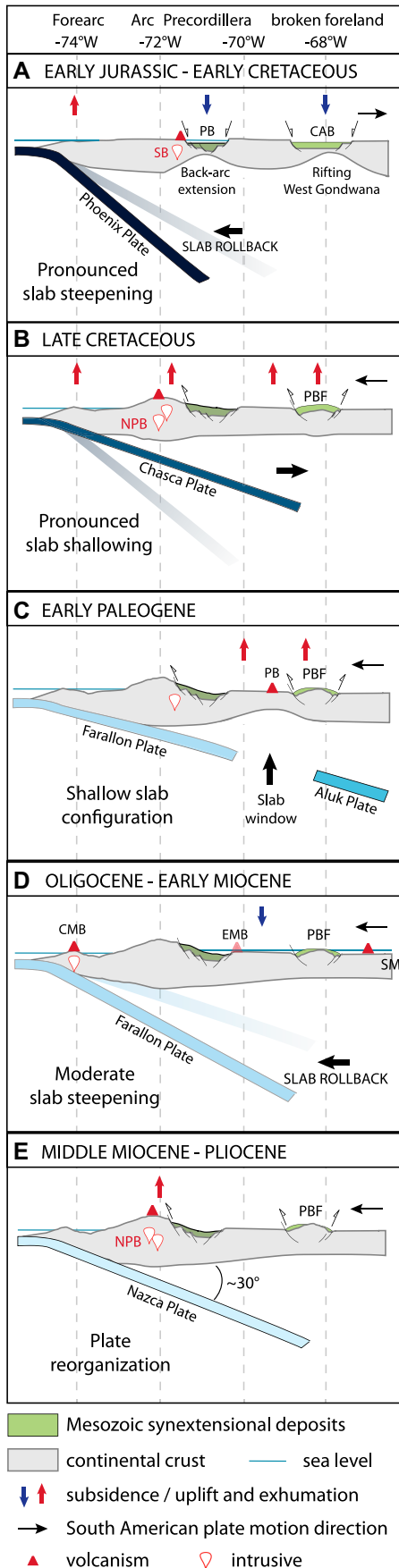


Figure 6. Cartoons show interpreted geodynamic evolution and migrations of the magmatism revealing slab geometry variations. (A) Regional subsidence linked to pronounced slab rollback and Gondwana rifting during Jurassic–Early Cretaceous times (PB—Piltriquitrón Basin, CAB—Cañadon Asfalto Basin, SB—Subcordilleran Batholith). (B) Late Cretaceous shallowing of the subducting slab and increase of plate coupling (PBF—Patagonian Broken Foreland, NPB—North Patagonian Batholith). (C) Paleogene opening of a slab window, enhancing uplift of the overriding plate (PB—Pilcaniyeu Belt). (D) Arc retreating to the trench between the Oligocene (EMB—El Maitén Belt) and the early Miocene (CMB—coastal magmatic belt) coeval with distal retroarc volcanism (SM—Somuncura plateau) and retroarc quiescence to moderate subsidence from the late Paleogene to the early Miocene. (E) Increased interplate coupling induced by plate reorganization, triggering exhumation of the Patagonian Precordillera (and possibly modest deformation of the broken foreland).

the Gastre-Navidad area yielded AHe ages spanning through the early Eocene and the Oligocene (Savignano et al., 2016). However, discrepancies among replicates make a reliable evaluation of thermal history not possible.

The lack of late Eocene–early Miocene exhumation both in the foreland and in the mountain range is a clear signal of tectonic quiescence—or even local subsidence—which we relate to plate decoupling due to the onset of slab rollback and re-steepening of the subduction geometry (Fig. 6E). This was induced by a sharp reduction in average trenchward velocity and/or by subduction of the former oceanic segment of the Farallon plate and a related decrease in buoyancy (Aragón et al., 2011; Maloney et al., 2013). Coeval retroarc magmatism was widespread (Pilcaniyeu Belt, El Maitén Belt, and Somuncura Plateau; De Ignacio et al., 2001; Echaurren et al., 2016; Iannelli et al., 2018).

Cooling ages and thermal histories derived from thermal modeling indicate distinct evolution patterns for the Andean chain and the broken foreland during the Neogene. Indeed, middle Miocene–Pliocene exhumation is solely recorded by our data in the Patagonian Precordillera, although the cooling pattern is not homogeneous throughout the area investigated. In fact, a few samples collected from sub-volcanic bodies show a rapid cooling following emplacement at shallow depths during the Cretaceous (Adriasola et al., 2006). Other samples were affected at the

same time by minor heating, which was possibly related to the intrusion of the North Patagonia Batholith. While Late Cretaceous–Paleocene regional shortening was related to flat-slab subduction, Neogene deformation in the Patagonian Precordillera occurred without major changes in the subduction geometry (Echaurren et al., 2019). Plate coupling increase at this time was rather controlled by plate reorganization due to higher convergence rates and a mostly orthogonal subduction induced by the break-up of the Farallon Plate at ca. 23 Ma (Somoza, 1998; Lonsdale, 2005). On the other hand, our data do not record any significant Neogene exhumation in the broken foreland. Although substantial middle Miocene–Pliocene shortening was also suggested in this sector (Bilmes et al., 2013), the lack of any thermochronology signal since the Paleogene confirms that Neogene deformation was minor (Savignano et al., 2016) and unable to produce significant vertical movement. Based on inverse modeling, we propose that the thermal history of the foreland over the last 70 m.y. was characterized by regional cooling that was not affected by any particular thermal and/or important deformation event (with the exception of a few local areas characterized by some heating related to volcanic activity). Available low-temperature thermochronological data from the southern Andean foreland at 47–49°S (Deseado Massif; Fernández et al., 2020) suggest that such a nearly steady-state slow cooling may have characterized the whole Patagonian foreland since the Late Cretaceous.

CONCLUSIONS

AFT and AHe data, as well as temperature-time history modeling, suggest spatio-temporal variations of exhumation associated with alternating phases of plate-scale regional shortening and tectonic quiescence in Patagonia. Kilometer-scale subsidence during the Jurassic resulted from protracted slab rollback and a rifting phase in the eastern retroarc. Exhumation of the Patagonian Precordillera and the broken foreland related to slab shallowing started during late Early Cretaceous to Paleocene times and was enhanced by the deformation of preexisting grabens located between the Patagonian Andes and the North Patagonian Massif. Thermochronological data in the foreland show minor subsidence from late Eocene to early Miocene times. A marked contrast is observed between the broken foreland samples, which were already at low temperatures during the Paleogene, and the Precordilleran granite samples, which were affected by a late reheating phase that was possibly linked to Miocene arc magmatism. Middle Miocene–Pliocene exhumation is then exclusively recorded in the

Andean chain, whereas coeval deformation in the broken foreland was rather limited and anyway insufficient to produce noticeable exhumation. Besides allowing us to define the articulated exhumation pattern characterizing the Andean orogen and its foreland between 40°S and 45°S, altogether our results unravel with unprecedented resolution the significant magnitude of Jurassic to Early Cretaceous burial and Late Cretaceous to present unroofing of northern Patagonia.

ACKNOWLEDGMENTS

Funding for this work was provided by the University of Padova (Progetto di Ateneo 2015, CPDA158355) and the Universidad Nacional de Río Negro (PICT-FONCyT 2013-2916, PIP-CONICET 330, U.N. Comahue). S. Boesso, R. Pinna, and L. Bordier are thanked for sample preparation and for their assistance during the analyses. The thoughtful and constructive review by B. Horton and the useful comments of the associate editor are gratefully acknowledged. B. Guillaume is thanked for his useful comments.

REFERENCES CITED

- Adriasola, A.C., Thomson, S.N., Brix, M.R., Hervé, F., and Stöckhert, B., 2006, Postmagmatic cooling and late Cenozoic denudation of the North Patagonian Batholith in the Los Lagos region of Chile, 41–42 15' S: *International Journal of Earth Sciences*, v. 95, p. 504–528, <https://doi.org/10.1007/s00531-005-0027-9>.
- Anselmi, G., Gamba, M.T., and Panza, J.L.A., 2004, Hoja Geológica 4369-IV Los Altares: Servicio Geológico Minero Argentino. Instituto de Geología y Recursos Minerales.
- Aragón, E., D'Eramo, F., Castro, A., Pinotti, L., Brunelli, D., Rabbia, O., Rivalenti, G., Varela, R., Spakman, W., and Demartis, M., 2011, Tectono-magmatic response to major convergence changes in the North Patagonian suprasubduction system; the Paleogene subduction–transcurrent plate margin transition: *Tectonophysics*, v. 509, p. 218–237, <https://doi.org/10.1016/j.tecto.2011.06.012>.
- Aragón, E., Pinotti, L., Fernando, D., Castro, A., Rabbia, O., Coniglio, J., Demartis, M., Hernando, I., Cavarozzi, C.E., and Aguilera, Y.E., 2013, The Farallon-Aluk ridge collision with South America: Implications for the geochemical changes of slab window magmas from fore- to back-arc: *Geoscience Frontiers*, v. 4, p. 377–388, <https://doi.org/10.1016/j.gsf.2012.12.004>.
- Ardolino, A., Lizuain, A., Salani, F., and Pezzuchi, H., 2011, Mapa geológico preliminar de la Hoja 4369-II: Gan Gan, provincia del Chubut. Programa Nacional de Cartas Geológicas de la República Argentina, escala, v. 1.
- Ávila, P., and Dávila, F.M., 2020, Lithospheric thinning and dynamic uplift effects during slab window formation, southern Patagonia (45°–55° S): *Journal of Geodynamics*, v. 133, no. 101689, <https://doi.org/10.1016/j.jog.2019.101689>.
- Bilmes, A., D'Elia, L., Franzese, J.R., Veiga, G.D., and Hernández, M., 2013, Miocene block uplift and basin formation in the Patagonian foreland: The Gastre Basin, Argentina: *Tectonophysics*, v. 601, p. 98–111, <https://doi.org/10.1016/j.tecto.2013.05.001>.
- Bishop, B.T., Beck, S.L., Zandt, G., Wagner, L.S., Long, M.D., and Tavera, H., 2018, Foreland uplift during flat subduction: Insights from the Peruvian Andes and Fitzcarrald Arch: *Tectonophysics*, v. 731, p. 73–84, <https://doi.org/10.1016/j.tecto.2018.03.005>.
- Burtner, R.L., Nigrini, A., and Donelick, R.A., 1994, Thermochronology of Lower Cretaceous source rocks in the Idaho–Wyoming thrust belt: *American Association of Petroleum Geologists Bulletin*, v. 78, p. 1613–1636.
- Butler, K.L., Horton, B.K., Echaurren, A., Folguera, A., and Fuentes, F., 2020, Cretaceous–Cenozoic growth of the Patagonian broken foreland basin, Argentina: Chronostratigraphic framework and provenance variations during transitions in Andean subduction dynamics: *Journal of South American Earth Sciences*, v. 97, no. 102242, <https://doi.org/10.1016/j.jsames.2019.102242>.
- Cerpa, N.G., Guillaume, B., and Martinod, J., 2018, The interplay between overriding plate kinematics, slab dip and tectonics: *Geophysical Journal International*, v. 215, p. 1789–1802, <https://doi.org/10.1093/gji/ggy365>.
- Cesari, O., 1977, Informe de ensayo inicial del pozo YPF. Ch. PRM. es-I. Sección: Consideraciones estratigráficas: Unpublished report of YPF.
- Charrier, R., Pinto, L., and Rodríguez, M.P., 2007, Tectonostratigraphic evolution of the Andean Orogen in Chile, in Moreno, T., and Gibbons, W., *The Geology of Chile*: London, UK, Geological Society, London, p. 21–114.
- Cloos, M., 1993, Lithospheric buoyancy and collisional orogenesis: Subduction of oceanic plateaus, continental margins, island arcs, spreading ridges, and seamounts: *Geological Society of America Bulletin*, v. 105, p. 715–737, [https://doi.org/10.1130/0016-7606\(1993\)105<0715:LBACOS>2.3.CO;2](https://doi.org/10.1130/0016-7606(1993)105<0715:LBACOS>2.3.CO;2).
- Cobbold, P.R., and Rossello, E.A., 2003, Aptian to recent compressional deformation, foothills of the Neuquén Basin, Argentina: *Marine and Petroleum Geology*, v. 20, p. 429–443, [https://doi.org/10.1016/S0264-8172\(03\)00077-1](https://doi.org/10.1016/S0264-8172(03)00077-1).
- Coira, B., Kay, S.M., and Viramonte, J., 1993, Upper Cenozoic magmatic evolution of the Argentine Puna—A model for changing subduction geometry: *International Geology Review*, v. 35, p. 677–720, <https://doi.org/10.1080/00206819309465552>.
- Cucchi, R.J., Busteros, A.G., Lema, H.A., Dalponte, M.R., Espejo, P.M., and Franchi, M., 2001, Hoja Geológica 4169-II Los Menucos: Servicio Geológico Minero Argentino, Instituto de Geología y Recursos Minerales.
- Cucchi, R.J., Espejo, P.M., and González, R., 1998, Hoja Geológica 4169-I, Piedra del Águila, provincias del Neuquén y Río Negro, Programa Nacional de Cartas Geológicas de la República Argentina, scale 1:250,000: SEGEMAR (Buenos Aires, Servicio Geológico Minero Argentino. Instituto de Geología y Recursos Minerales) Boletín—Instituto de Estudios de Población y Desarrollo (Dominican Republic), v. 242, p. 1–74.
- Cúneo, R., Ramezani, J., Scasso, R., Pol, D., Escapa, I., Zavattieri, A.M., and Bowring, S.A., 2013, High-precision U–Pb geochronology and a new chronostratigraphy for the Cañadón Asfalto Basin, Chubut, central Patagonia: Implications for terrestrial faunal and floral evolution in Jurassic: *Gondwana Research*, v. 24, p. 1267–1275, <https://doi.org/10.1016/j.gr.2013.01.010>.
- De Ignacio, C., López, I., Oyarzun, R., and Márquez, A., 2001, The northern Patagonia Somuncura plateau basalts: A product of slab-induced, shallow asthenospheric upwelling?: *Terra Nova*, v. 13, p. 117–121, <https://doi.org/10.1046/j.1365-3121.2001.00326.x>.
- Dunkl, I., 2002, TRACKKEY: A Windows program for calculation and graphical presentation of fission track data: *Computers & Geosciences*, v. 28, p. 3–12, [https://doi.org/10.1016/S0098-3004\(01\)00024-3](https://doi.org/10.1016/S0098-3004(01)00024-3).
- Eagles, G., 2007, New angles on South Atlantic opening: *Geophysical Journal International*, v. 168, p. 353–361, <https://doi.org/10.1111/j.1365-246X.2006.03206.x>.
- Echaurren, A., Folguera, A., Gianni, G., Orts, D., Tassara, A., Encinas, A., Giménez, M., and Valencia, V., 2016, Tectonic evolution of the North Patagonian Andes (41°–44°S) through recognition of syntectonic strata: *Tectonophysics*, v. 677, p. 99–114, <https://doi.org/10.1016/j.tecto.2016.04.009>.
- Echaurren, A., Oliveros, V., Folguera, A., Ibarra, F., Creixell, C., and Lucassen, F., 2017, Early Andean tectonomagmatic stages in north Patagonia: Insights from field and geochemical data: *Journal of the Geological Society*, v. 174, p. 405–421, <https://doi.org/10.1144/jgs2016-087>.
- Echaurren, A., Lucía, F.P., Navarrete, C., Verónica, O., Encinas, A., Mario, G., Lince-Klinger, F., and Andrés, F., 2019, Tectonic controls on the building of the North Patagonian fold-thrust belt (~43° S), in Horton, B., and Folguera, A., eds., *Andean Tectonics*: Elsevier, p. 609–650.
- Encinas, A., Folguera, A., Oliveros, V., Del Mauro, L.D.G., Tapia, F., Riffo, R., Hervé, F., Finger, K.L., Valencia, V.A., and Gianni, G., 2016, Late Oligocene–early Miocene submarine volcanism and deep-marine sedimentation in an extensional basin of southern Chile: Implications for the tectonic development of the North Patagonian Andes: *Geological Society of America Bulletin*, v. 128, p. 807–823, <https://doi.org/10.1130/B31303.1>.
- England, P., Engdahl, R., and Thatcher, W., 2004, Systematic variation in the depths of slabs beneath arc volcanoes: *Geophysical Journal International*, v. 156, p. 377–408, <https://doi.org/10.1111/j.1365-246X.2003.02132.x>.
- Escosteguy, L.D., Geuna, S.E., Franchi, M., González Díaz, E.F., Dal Molin, C.N., Etcheverría, M.P., Cegarra, M.I., Wilson, C., and González, R., 2013, Hoja Geológica 4172-II San Martín de los Andes: Servicio Geológico Minero Argentino, Instituto de Geología y Recursos Minerales.
- Fan, M., and Carrapa, B., 2014, Late Cretaceous–early Eocene Laramide uplift, exhumation, and basin subsidence in Wyoming: Crustal responses to flat slab subduction: *Tectonics*, v. 33, p. 509–529, <https://doi.org/10.1002/2012TC003221>.
- Fernández, M.L., Mazzoli, S., Zattin, M., Savignano, E., Genge, M.C., Tavani, S., Garrone, A., and Franchini, M., 2020, Structural controls on Jurassic gold mineralization, and Cretaceous–Tertiary exhumation in the foreland of the southern Patagonian Andes: New constraints from La Paloma area, Deseado Massif, Argentina: *Tectonophysics*, v. 775, no. 228302, <https://doi.org/10.1016/j.tecto.2019.228302>.
- Fernández Paz, L., Bechis, F., Litvak, V.D., Echaurren, A., Encinas, A., González, J., Lucassen, F., Oliveros, V., Valencia, V., and Folguera, A., 2019, Constraints on trenchward arc migration and backarc magmatism in the North Patagonian Andes in the context of Nazca Plate Rollback: *Tectonics*, v. 38, p. 3794–3817, <https://doi.org/10.1029/2019TC005580>.
- Figari, E.G., Scasso, R.A., Cúneo, R.N., and Escapa, I., 2015, Stratigraphy and geologic evolution of the Cañadón Asfalto Basin, Chubut Province, Argentina: *Latin American Journal of Sedimentology and Basin Analysis*, v. 22, p. 135–169.
- Fillon, C., Gautheron, C., and van der Beek, P., 2013, Oligocene–Miocene burial and exhumation of the Southern Pyrenean foreland quantified by low-temperature thermochronology: *Journal of the Geological Society*, v. 170, p. 67–77, <https://doi.org/10.1144/jgs2012-051>.
- Finzel, E.S., Trop, J.M., Ridgway, K.D., and Enkelmann, E., 2011, Upper plate proxies for flat-slab subduction processes in southern Alaska: *Earth and Planetary Science Letters*, v. 303, p. 348–360, <https://doi.org/10.1016/j.epsl.2011.01.014>.
- Flowers, R.M., Ketchum, R.A., Shuster, D.L., and Farley, K.A., 2009, Apatite (U–Th)/He thermochronometry using a radiation damage accumulation and annealing model: *Geochimica et Cosmochimica Acta*, v. 73, p. 2347–2365, <https://doi.org/10.1016/j.gca.2009.01.015>.
- Folguera, A., and Iannizzotto, N.F., 2004, The lagos La Plata and Fontana fold-and-thrust belt: Long-lived orogenesis at the edge of western Patagonia: *Journal of South American Earth Sciences*, v. 16, p. 541–566, <https://doi.org/10.1016/j.jsames.2003.10.001>.
- Folguera, A., and Ramos, V.A., 2011, Repeated eastward shifts of arc magmatism in the Southern Andes: A revision to the long-term pattern of Andean uplift and magmatism: *Journal of South American Earth Sciences*, v. 32, p. 531–546, <https://doi.org/10.1016/j.jsames.2011.04.003>.
- Folguera, A., Encinas, A., Echaurren, A., Gianni, G., Orts, D., Valencia, V., and Carrasco, G., 2018, Constraints on the Neogene growth of the central Patagonian Andes at the latitude of the Chile triple junction (45–47 S) using U/Pb geochronology in synorogenic strata: *Tectonophysics*, v. 744, p. 134–154, <https://doi.org/10.1016/j.tecto.2018.06.011>.
- Gabaldón, V., 1982, Estratigrafía y sedimentología del Liásico del noroeste del Chubut, Argentina: Buenos Aires, Actas 5° Congreso Latinoamericano de Geología, v. 2, p. 509–526.
- Galbraith, R.F., and Laslett, G.M., 1993, Statistical models for mixed fission track ages: *Nuclear Tracks and Radiation Measurements*, v. 21, p. 459–470.

- Gallagher, K., 2012, Transdimensional inverse thermal history modeling for quantitative thermochronology: *Journal of Geophysical Research: Solid Earth*, v. 117, <https://doi.org/10.1029/2011JB008825>.
- Gallagher, K., Charvin, K., Nielsen, S., Sambridge, M., and Stephenson, J., 2009, Markov chain Monte Carlo (MCMC) sampling methods to determine optimal models, model resolution and model choice for Earth Science problems: *Marine and Petroleum Geology*, v. 26, p. 525–535, <https://doi.org/10.1016/j.marpetgeo.2009.01.003>.
- Gautheron, C., Tassan-Got, L., Barbarand, J., and Pagel, M., 2009, Effect of alpha-damage annealing on apatite (U-Th)/He thermochronology: *Chemical Geology*, v. 266, p. 157–170, <https://doi.org/10.1016/j.chemgeo.2009.06.001>.
- Gautheron, C., and Tassan-Got, L., 2010, A Monte Carlo approach to diffusion applied to noble gas/helium thermochronology: *Chemical Geology*, v. 273, p. 212–224, <https://doi.org/10.1016/j.chemgeo.2010.02.023>.
- Gautheron, C., Barbarand, J., Ketcham, R.A., Tassan-Got, L., van der Beek, P., Pagel, M., Pinna-Jamme, R., Couffignal, F., and Fialin, M., 2013, Chemical influence on α -recoil damage annealing in apatite: Implications for (U-Th)/He dating: *Chemical Geology*, v. 351, p. 257–267, <https://doi.org/10.1016/j.chemgeo.2013.05.027>.
- George, S.W., Davis, S.N., Fernández, R.A., Manríquez, L.M., Leppe, M.A., Horton, B.K., and Clarke, J.A., 2020, Chronology of deposition and unconformity development across the Cretaceous–Paleogene boundary, Magallanes–Austral Basin, Patagonian Andes: *Journal of South American Earth Sciences*, v. 97, no. 102237, <https://doi.org/10.1016/j.jsames.2019.102237>.
- Ghiorzi, A., 1979, Informe final de pozo YPF. Ch. Ca. es-I. Section: Geología: Unpublished report of YPF.
- Giacosa, R.E., and Heredia, N., 2004, Estructura de los Andes Nordpatagónicos en los cordones Piltriquitrón y Serrucho y en el valle de El Bolsón (41° 30'–42° 00' S), Río Negro: *Revista de la Asociación Geológica Argentina*, v. 59, p. 91–102.
- Giacosa, R.E., Heredia Carballo, N., Zubía, M.A., González, R., Faroux, A.J., Césari, O., and Franchi, M., 2001, Hoja geológica 4172-IV San Carlos de Bariloche: Servicio Geológico Minero Argentino, Instituto de Geología y Recursos Minerales.
- Gianni, G., Navarrete, C., Orts, D., Toba, J., Folguera, A., and Giménez, M., 2015, Patagonian broken foreland and related synorogenic rifting: The origin of the Chubut Group Basin: *Tectonophysics*, v. 649, p. 81–99, <https://doi.org/10.1016/j.tecto.2015.03.006>.
- Gianni, G.M., Echaurren, A., Folguera, A., Likerman, J., Encinas, A., García, H.P.A., Dal Molin, C., and Valencia, V.A., 2017, Cenozoic intraplate tectonics in Central Patagonia: Record of main Andean phases in a weak upper plate: *Tectonophysics*, v. 721, p. 151–166, <https://doi.org/10.1016/j.tecto.2017.10.005>.
- Gianni, G.M., Dávila, F.M., Echaurren, A., Fennell, L., Toba, J., Navarrete, C., Quezada, P., Folguera, A., and Giménez, M., 2018, A geodynamic model linking Cretaceous orogeny, arc migration, foreland dynamic subsidence and marine incision in southern South America: *Earth-Science Reviews*, v. 185, p. 437–462, <https://doi.org/10.1016/j.earscirev.2018.06.016>.
- Gleadow, A.J.W., 1981, Fission-track dating methods: What are the real alternatives?: *Nuclear Tracks*, v. 5, p. 3–14, [https://doi.org/10.1016/0191-278X\(81\)90021-4](https://doi.org/10.1016/0191-278X(81)90021-4).
- González, P., Dalponte, M., Coluccia, A., Franchi, M., and Caba, R., 2000, Ingeniero Jacobacci, Programa Nacional de Cartas Geológicas de la República Argentina, scale 1:250,000, Hoja Geológica 4169-III: Provincia de Río Negro (Buenos Aires, Servicio Geológico Minero Argentino, Instituto de Geología y Recursos Minerales): Boletín - Instituto de Estudios de Población y Desarrollo (Dominican Republic), p. 311.
- Gordon, A., and Ort, M.H., 1993, Edad y correlación del plutonismo subcordillerano en las provincias de Río Negro y Chubut (41–42° 30' LS): *Congreso Geológico Argentino*, v. 12, p. 120–127.
- Green, P.F., Duddy, I.R., Laslett, G.M., Hegarty, K.A., Gleadow, A.W., and Lovering, J.F., 1989, Thermal annealing of fission tracks in apatite 4. Quantitative modelling techniques and extension to geological timescales: *Chemical Geology. Isotope Geoscience Section*, v. 79, p. 155–182, [https://doi.org/10.1016/0168-9622\(89\)90018-3](https://doi.org/10.1016/0168-9622(89)90018-3).
- Guillaume, B., Martinod, J., Husson, L., Roddaz, M., and Riquelme, R., 2009, Neogene uplift of central eastern Patagonia: Dynamic response to active spreading ridge subduction?: *Tectonics*, v. 28, <https://doi.org/10.1029/2008TC002324>.
- Gutscher, M.-A., 2002, Andean subduction styles and their effect on thermal structure and interplate coupling: *Journal of South American Earth Sciences*, v. 15, p. 3–10, [https://doi.org/10.1016/S0895-9811\(02\)00002-0](https://doi.org/10.1016/S0895-9811(02)00002-0).
- Gutscher, M.-A., and Peacock, S.M., 2003, Thermal models of flat subduction and the rupture zone of great subduction earthquakes: *Journal of Geophysical Research: Solid Earth*, v. 108, p. ESE 2-1–ESE 2-16.
- Gutscher, M.-A., Spakman, W., Bijwaard, H., and Engdahl, E.R., 2000, Geodynamics of flat subduction: Seismicity and tomographic constraints from the Andean margin: *Tectonics*, v. 19, p. 814–833, <https://doi.org/10.1029/1999TC001152>.
- Haller, M.J.F., Lech, R.R., Martínez, O., Meister, C.M., Poma, S., and Viera, R.L.M., 2010, Hoja Geológica 4372-III/IV Trevelin: Servicio Geológico Minero Argentino, Instituto de Geología y Recursos Minerales.
- Hamza, V.M., and Muñoz, M., 1996, Heat flow map of South America: *Geothermics*, v. 25, p. 599–646, [https://doi.org/10.1016/S0375-6505\(96\)00025-9](https://doi.org/10.1016/S0375-6505(96)00025-9).
- Horton, B.K., 2018, Tectonic regimes of the central and southern Andes: Responses to variations in plate coupling during subduction: *Tectonics*, v. 37, p. 402–429, <https://doi.org/10.1002/2017TC004624>.
- Horton, B.K., and Fuentes, F., 2016, Sedimentary record of plate coupling and decoupling during growth of the Andes: *Geology*, v. 44, p. 647–650, <https://doi.org/10.1130/G37918.1>.
- Horton, B.K., Fuentes, F., Boll, A., Starck, D., Ramirez, S.G., and Stockli, D.F., 2016, Andean stratigraphic record of the transition from backarc extension to orogenic shortening: A case study from the northern Neuquén Basin, Argentina: *Journal of South American Earth Sciences*, v. 71, p. 17–40, <https://doi.org/10.1016/j.jsames.2016.06.003>.
- Hurford, A.J., and Green, P.F., 1983, The zeta age calibration of fission-track dating: *Chemical Geology*, v. 41, p. 285–317, [https://doi.org/10.1016/S0009-2541\(83\)80026-6](https://doi.org/10.1016/S0009-2541(83)80026-6).
- Iannelli, S.B., Paz, L.F., Litvak, V.D., Jones, R.E., Ramos, M.E., Folguera, A., and Ramos, V.A., 2018, Paleogene arc-related volcanism in the southern central Andes and north Patagonia (39–41° S), in Folguera, A., ed., *The Evolution of the Chilean-Argentinean Andes*: Springer, p. 343–359.
- Jordán, T.E., Isaacs, B.L., Allmendinger, R.W., Brewer, J.A., Ramos, V.A., and Ando, C.J., 1983, Andean tectonics related to geometry of subducted Nazca plate: *Geological Society of America Bulletin*, v. 94, p. 341–361, [https://doi.org/10.1130/0016-7606\(1983\)94<341:ATR TGO>2.0.CO;2](https://doi.org/10.1130/0016-7606(1983)94<341:ATR TGO>2.0.CO;2).
- Kay, S.M., Godoy, E., and Kurtz, A., 2005, Episodic arc migration, crustal thickening, subduction erosion, and magmatism in the south-central Andes: *Geological Society of America Bulletin*, v. 117, p. 67–88, <https://doi.org/10.1130/B25431.1>.
- Kay, S.M., Ardolino, A.A., Gorrin, M.L., and Ramos, V.A., 2007, The Somuncura Large Igneous Province in Patagonia: Interaction of a transient mantle thermal anomaly with a subducting slab: *Journal of Petrology*, v. 48, p. 43–77, <https://doi.org/10.1093/petrology/egl053>.
- Ketcham, R.A., Carter, A., Donelick, R.A., Barbarand, J., and Hurford, A.J., 2007, Improved modeling of fission-track annealing in apatite: *The American Mineralogist*, v. 92, p. 799–810, <https://doi.org/10.2138/am.2007.2281>.
- Ketcham, R.A., Gautheron, C., and Tassan-Got, L., 2011, Accounting for long alpha-particle stopping distances in (U-Th-Sm)/He geochronology: Refinement of the baseline case: *Geochimica et Cosmochimica Acta*, v. 75, p. 7779–7791, <https://doi.org/10.1016/j.gca.2011.10.011>.
- Kraml, M., Pik, R., Rahn, M., Selbekk, R., Carignan, J., and Keller, J., 2006, A new multi-mineral age reference material for $^{40}\text{Ar}/^{39}\text{Ar}$ -(U-Th)/He and fission track dating methods: The Limberg t3 tuff: *Geostandards and Geoanalytical Research*, v. 30, p. 73–86, <https://doi.org/10.1111/j.1751-908X.2006.tb00914.x>.
- Lallemand, S., Heuret, A., and Boutelier, D., 2005, On the relationships between slab dip, back-arc stress, upper plate absolute motion, and crustal nature in subduction zones: *Geochemistry, Geophysics, Geosystems*, v. 6, <https://doi.org/10.1029/2005GC000917>.
- Lizuaín, A., and Silva Nieto, D., 2011, Hoja 4369-I, Gastre, Provincia del Chubut: Instituto de Geología y Recursos Minerales: Servicio Geológico Minero Argentino, scale 1:250,000.
- Lizuaín, A., Viera, R.L.M., and Franchi, M., 2010, Hoja Geológica 4372-I y II Esquel: Servicio Geológico Minero Argentino, Instituto de Geología y Recursos Minerales.
- Lonsdale, P., 2005, Creation of the Cocos and Nazca plates by fission of the Farallon plate: *Tectonophysics*, v. 404, p. 237–264, <https://doi.org/10.1016/j.tecto.2005.05.011>.
- López, M., García, M., Bucher, J., Funes, D.S., D'Elia, L., Bilmes, A., Naipauer, M., Sato, A.M., Valencia, V.A., and Franzese, J.R., 2019, Structural evolution of the Collón Cura basin: Tectonic implications for the North Patagonian Broken Foreland: *Journal of South American Earth Sciences*, v. 93, p. 424–438, <https://doi.org/10.1016/j.jsames.2019.04.021>.
- Maksymowicz, A., and Tassara, A., 2018, The Geometry of the Continental Wedge and Its Relation to the Rheology and Seismicity of the Chilean Interplate Boundary, in Folguera, A., et al., eds., *The Evolution of the Chilean-Argentinean Andes*: Springer, p. 31–58, https://doi.org/10.1007/978-3-319-67774-3_2.
- Maloney, K.T., Clarke, G.L., Klepeis, K.A., and Quevedo, L., 2013, The Late Jurassic to present evolution of the Andean margin: Drivers and the geological record: *Tectonics*, v. 32, p. 1049–1065, <https://doi.org/10.1002/tect.20067>.
- Martinod, J., Husson, L., Roperch, P., Guillaume, B., and Espurt, N., 2010, Horizontal subduction zones, convergence velocity and the building of the Andes: *Earth and Planetary Science Letters*, v. 299, p. 299–309, <https://doi.org/10.1016/j.epsl.2010.09.010>.
- Mazzoni, M.M., Kawashita, K., Harrison, S., and Aragón, E., 1991, Edades radimétricas eocenas en el borde occidental del Macizo Norpatagónico: *Revista de la Asociación Geológica Argentina*, v. 46, p. 150–158.
- McDowell, F.W., McIntosh, W.C., and Farley, K.A., 2005, A precise $^{40}\text{Ar}/^{39}\text{Ar}$ reference age for the Durango apatite (U-Th)/He and fission-track dating standard: *Chemical Geology*, v. 214, p. 249–263, <https://doi.org/10.1016/j.chemgeo.2004.10.002>.
- McGeary, S., Nur, A., and Ben-Avraham, Z., 1985, Spatial gaps in arc volcanism: The effect of collision or subduction of oceanic plateaus: *Tectonophysics*, v. 119, p. 195–221, [https://doi.org/10.1016/0040-1951\(85\)90039-3](https://doi.org/10.1016/0040-1951(85)90039-3).
- Mescua, J.F., Giambiagi, L.B., and Ramos, V.A., 2013, Late Cretaceous uplift in the Malgüe fold-and-thrust belt (35° S), southern Central Andes of Argentina and Chile: *Andean Geology*, v. 40, p. 102–116, <https://doi.org/10.5027/andgeoV40n1-a05>.
- Mpodozis, C., and Ramos, V.A., 2008, Tectónica jurásica en Argentina y Chile: Extensión, subducción oblicua, rifting, deriva y colisiones?: *Revista de la Asociación Geológica Argentina*, v. 63, p. 481–497.
- Müller, R.D., Seton, M., Zahirovic, S., Williams, S.E., Matthews, K.J., Wright, N.M., Shephard, G.E., Maloney, K.T., Barnett-Moore, N., and Hosseinpour, M., 2016, Ocean basin evolution and global-scale plate reorganization events since Pangea breakup: *Annual Review of Earth and Planetary Sciences*, v. 44, p. 107–138, <https://doi.org/10.1146/annurev-earth-060115-012211>.
- Muñoz, M., 1999, Tectonophysics of the Andes region: Relationships with heat flow and the thermal structure, in *International Symposium on Andean Geodynamics*, p. 532–534.
- Murray, K.E., Orme, D.A., and Reiners, P.W., 2014, Effects of U-Th-rich grain boundary phases on apatite helium ages: *Chemical Geology*, v. 390, p. 135–151, <https://doi.org/10.1016/j.chemgeo.2014.09.023>.
- Navarrete, C., Gianni, G., Echaurren, A., Kingler, F.L., and Folguera, A., 2016, Episodic Jurassic to lower Cretaceous intraplate compression in Central Patagonia during Gondwana breakup: *Journal of Geodynamics*, v. 102, p. 185–201, <https://doi.org/10.1016/j.jjog.2016.10.001>.

- Navarrete, C.R., Gianni, G.M., Echaurren, A., and Folguera, A., 2018, Lower Jurassic to early Paleogene intraplate contraction in central Patagonia, *in* Folguera, A., et al., The Evolution of the Chilean-Argentinean Andes, Springer, p. 245–271, https://doi.org/10.1007/978-3-319-67774-3_10.
- Olivero, E.B., 1982, Estratigrafía de la cuenca sur del Lago Fontana [Ph.D. thesis]: Buenos Aires, Argentina, Universidad de Buenos Aires.
- Oncken, O., Chong, G., Franz, G., Giese, P., Götze, H.-J., Ramos, V.A., Strecker, M.R., and Wigger, P., 2006, The Andes: Active Subduction Orogeny: Berlin/Heidelberg, Germany, Springer Science & Business Media, <https://doi.org/10.1007/978-3-540-48684-8>.
- Orts, D.L., Folguera, A., Encinas, A., Ramos, M., Tobal, J., and Ramos, V.A., 2012, Tectonic development of the North Patagonian Andes and their related Miocene foreland basin (41° 30′–43° S): *Tectonics*, v. 31, <https://doi.org/10.1029/2011TC003084>.
- Orts, D.L., Folguera, A., Giménez, M., Ruiz, F., Vera, E.A.R., and Klinger, F.L., 2015, Cenozoic building and deformational processes in the North Patagonian Andes: *Journal of Geodynamics*, v. 86, p. 26–41, <https://doi.org/10.1016/j.jog.2015.02.002>.
- Page, S., and Page, R., 1999, Las diabasas y gabros del Jurásico de la Precordillera del Chubut: *Geológica Argentina. Servicio Geológico Minero Argentino, Instituto de Geología y Recursos Minerales: Anales*, v. 29, p. 489–495.
- Pankhurst, R.J., Hervé, F., Fanning, M., and Suárez, M., 2003, Coeval plutonic and volcanic activity in the Patagonian Andes: The Patagonian Batholith and the Ibáñez and Divisadero formations, Aysén, southern Chile, *in* Campos, E., ed., *Congreso Geológico Chileno (No. 10): Concepción, Actas CD-ROM*.
- Paz, L.F., Litvak, V.D., Echaurren, A., Iannelli, S.B., Encinas, A., Folguera, A., and Valencia, V., 2018, Late Eocene volcanism in North Patagonia (42°30′–43°S): Arc resumption after a stage of within-plate magmatism: *Journal of Geodynamics*, v. 113, p. 13–31, <https://doi.org/10.1016/j.jog.2017.11.005>.
- Pilger, R.H., Jr., 1981, Plate reconstructions, aseismic ridges, and low-angle subduction beneath the Andes: *Geological Society of America Bulletin*, v. 92, p. 448–456, [https://doi.org/10.1130/0016-7606\(1981\)92<448:PRA RAL>2.0.CO;2](https://doi.org/10.1130/0016-7606(1981)92<448:PRA RAL>2.0.CO;2).
- Ramos, M.E., Orts, D.L., Calatayud, F., Pazos, P.J., Folguera, T., Telichevsky, A., and Ramos, V.A., 2011, Estructura, Estratigrafía y evolución tectónica de la cuenca de Nirihuau en las nacientes del río Cushamen, Chubut: *Revista de la Asociación Geológica Argentina*, v. 68, no. 2, p. 210–224.
- Ramos, V., 1999, Plate tectonic setting of the Andean Cordillera: Episodes, v. 22, p. 183–190, <https://doi.org/10.18814/epiuius/1999/v22i3/005>.
- Ramos, V.A., 1981, Descripción geológica de la Hoja 47 Ab—Lago Fontana”, Provincia Del Chubut: Carta Geológica-económica de la República Argentina, escala 1: 200.000: Servicio Geológico Nacional, 183.
- Ramos, V.A., 2010, The tectonic regime along the Andes: Present-day and Mesozoic regimes: *Geological Journal*, v. 45, p. 2–25, <https://doi.org/10.1002/gj.1193>.
- Ramos, V.A., and Folguera, A., 2005, Tectonic evolution of the Andes of Neuquén: Constraints derived from the magmatic arc and foreland deformation, *in* Veiga, G.D., Spalletti, L.A., Howell, J.A., and Schwarz, E., eds., *The Neuquén Basin, Argentina: A Case Study in Sequence Stratigraphy and Basin Dynamics*: Geological Society, London, *Special Publication 252*, p. 15–35, <https://doi.org/10.1144/GSL.SP.2005.252.01.02>.
- Ramos, V.A., and Folguera, A., 2009, Andean flat-slab subduction through time, *in* Murphy, J.B., Keppie, J.D., and Hynes, A.J., eds., *Ancient Orogens and Modern Analogues*: Geological Society, London, *Special Publication 327*, p. 31–54, <https://doi.org/10.1144/SP327.3>.
- Ramos, V.A., Cristallini, E.O., and Pérez, D.J., 2002, The Pampean flat-slab of the Central Andes: *Journal of South American Earth Sciences*, v. 15, p. 59–78, [https://doi.org/10.1016/S0895-9811\(02\)00006-8](https://doi.org/10.1016/S0895-9811(02)00006-8).
- Ramos, M.E., Folguera, A., Fennell, L., Giménez, M., Litvak, V.D., Dzierma, Y., and Ramos, V.A., 2014, Tectonic evolution of the North Patagonian Andes from field and gravity data (39–40° S): *Journal of South American Earth Sciences*, v. 51, p. 59–75, <https://doi.org/10.1016/j.jsames.2013.12.010>.
- Rapela, C.W., Pankhurst, R.J., and Harrison, S.M., 1992, Triassic “Gondwana” granites of the Gastre district, north Patagonian massif: *Earth and Environmental Science Transactions of The Royal Society of Edinburgh*, v. 83, p. 291–304, <https://doi.org/10.1017/S0263593300007975>.
- Rapela, C.W., Spalletti, L.A., Merodio, J.C., and Aragón, E., 1988, Temporal evolution and spatial variation of early Tertiary volcanism in the Patagonian Andes (40°S–42°30′ S): *Journal of South American Earth Sciences*, v. 1, p. 75–88, [https://doi.org/10.1016/0895-9811\(88\)90017-X](https://doi.org/10.1016/0895-9811(88)90017-X).
- Ravazzoli, I.A., and Sesana, F.L., 1977, Descripción geológica de la Hoja 41c, Río Chico: Buenos Aires, Servicio Geológico Nacional Boletín, v. 148, 77 p.
- Remesal, M., Salani, F., Franchi, M., Ardolino, A.A., Dalponte, M.R., Espejo, P.M., and Lizuáin, A., 2001, Hoja Geológica, 4169, IV, Maquinchao. Provincia de Río Negro: Buenos Aires, Instituto de Geología y Recursos Minerales, Servicio Geológico Minero Argentino, Boletín, v. 312, 68 p.
- Rodríguez-González, J., Negrode, A.M., and Billen, M.L., 2012, The role of the overriding plate thermal state on slab dip variability and on the occurrence of flat subduction: *Geochemistry, Geophysics, Geosystems*, v. 13, <https://doi.org/10.1029/2011GC003859>.
- Sachse, V.F., Anka, Z., Littke, R., Rodríguez, J.F., Horsfield, B., and di Primio, R., 2016, Burial, temperature and maturation history of the Austral and western Malvinas basins, southern Argentina, based on 3D basin modeling: *Journal of Petroleum Geology*, v. 39, p. 169–191, <https://doi.org/10.1111/jpg.12639>.
- Savignano, E., Mazzoli, S., Arce, M., Franchini, M., Gautheron, C., Paolini, M., and Zattin, M., 2016, (Un) Coupled thrust belt-foreland deformation in the northern Patagonian Andes: New insights from the Esquel-Gastre sector (41° 30′–43° S): *Tectonics*, v. 35, p. 2636–2656, <https://doi.org/10.1002/2016TC004225>.
- Schellart, W.P., 2017, Andean mountain building and magmatic arc migration driven by subduction-induced whole mantle flow: *Nature Communications*, v. 8, p. 1–13, <https://doi.org/10.1038/s41467-017-01847-z>.
- Schellart, W.P., 2020, Control of subduction zone age and size on flat slab subduction: *Frontiers of Earth Science*, v. 8, p. 1–18.
- Seipold, U., 1998, Temperature dependence of thermal transport properties of crystalline rocks—a general law: *Tectonophysics*, v. 291, p. 161–171, [https://doi.org/10.1016/S0040-1951\(98\)00037-7](https://doi.org/10.1016/S0040-1951(98)00037-7).
- Seton, M., Müller, R.D., Zahirovic, S., Gaina, C., Torsvik, T., Shephard, G., Talsma, A., Gurnis, M., Turner, M., and Maus, S., 2012, Global continental and ocean basin reconstructions since 200 Ma: *Earth-Science Reviews*, v. 113, p. 212–270, <https://doi.org/10.1016/j.earscirev.2012.03.002>.
- Silva Nieto, D.G., Márquez, M.J., Ardolino, A.A., and Franchi, M., 2005, Hoja Geológica 4369-III Paso de Indios: Servicio Geológico Minero Argentino, Instituto de Geología y Recursos Minerales.
- Silver, P.G., Russo, R.M., and Lithgow-Bertelloni, C., 1998, Coupling of South American and African plate motion and plate deformation: *Science*, v. 279, no. 5347, p. 60–63, <https://doi.org/10.1126/science.279.5347.60>.
- Skarmeta, J., 1976, Evolución tectónica y paleogeográfica de los Andes Patagónicos de Aisén durante el Neocósmio, *in* I Congreso Geológico Chileno (Santiago), v. 1, p. 1–56.
- Somoza, R., 1998, Updated azca (Farallon)—South America relative motions during the last 40 My: Implications for mountain building in the central Andean region: *Journal of South American Earth Sciences*, v. 11, p. 211–215, [https://doi.org/10.1016/S0895-9811\(98\)00012-1](https://doi.org/10.1016/S0895-9811(98)00012-1).
- Spagnuolo, M.G., Folguera, A., Litvak, V., Vera, E.A.R., and Ramos, V.A., 2012, Late Cretaceous arc rocks in the Andean retroarc region at 36.5°S: Evidence supporting a Late Cretaceous slab shallowing: *Journal of South American Earth Sciences*, v. 38, p. 44–56, <https://doi.org/10.1016/j.jsames.2012.05.002>.
- Suárez, M., and De la Cruz, R., 2001, Jurassic to Miocene K–Ar dates from eastern central Patagonian Cordillera plutons, Chile (45–48°S): *Geological Magazine*, v. 138, p. 53–66, <https://doi.org/10.1017/S0016756801004903>.
- Suarez, M., and Marquez, M., 2007, A Torcisan retro-arc basin of Central Patagonia (Chubut), Argentina: Middle Jurassic closure, arc migration and tectonic setting: *Andean Geology*, v. 34, p. 63–79, <https://doi.org/10.5027/andgeoV34n1-a04>.
- Suárez, M., Márquez, M., De La Cruz, R., and Fanning, M., 2009, Apatian-Albian subaerial volcanic rocks in central Patagonia: Divisadero and Chubut Groups, *in* XII Congreso Geológico Chileno, p. 1–4.
- Syracuse, E.M., and Abers, G.A., 2006, Global compilation of variations in slab depth beneath arc volcanoes and implications: *Geochemistry, Geophysics, Geosystems*, v. 7, <https://doi.org/10.1029/2005GC001045>.
- Thomson, S.N., 2002, Late Cenozoic geomorphic and tectonic evolution of the Patagonian Andes between latitudes 42°S and 46°S: An appraisal based on fission-track results from the transpressional intra-arc Liquiñe-Ofqui fault zone: *Geological Society of America Bulletin*, v. 114, p. 1159–1173, [https://doi.org/10.1130/0016-7606\(2002\)114<1159:LCGATE>2.0.CO;2](https://doi.org/10.1130/0016-7606(2002)114<1159:LCGATE>2.0.CO;2).
- Thomson, S.N., Brandon, M.T., Tomkin, J.H., Reiners, P.W., Vásquez, C., and Wilson, N.J., 2010, Glaciation as a destructive and constructive control on mountain building: *Nature*, v. 467, p. 313–317, <https://doi.org/10.1038/nature09365>.
- Turner, J.C., 1965, Estratigrafía de Aluminé y adyacencias, provincia de Neuquén: *Revista de la Asociación Geológica Argentina*, v. 20, p. 153–184.
- Varela, R., Basei, M.A., Cingolani, C.A., Siga, O., Jr., and Passarelli, C.R., 2005, El basamento cristalino de los Andes norpatagónicos en Argentina: *Geocronología e interpretación tectónica*: *Revista Geológica de Chile*, v. 32, p. 167–187, <https://doi.org/10.4067/S0716-02082005000200001>.
- Volckheimer, V., 1964, Estratigrafía de la zona extraandina del departamento de Cushamen (Chubut) entre los paralelos 42°00′ y 43°30′ y los meridianos 70°00′ y 71°00′: *Revista de la Asociación Geológica Argentina*, v. 19, p. 85–107.
- von Gosen, W., and Loske, W., 2004, Tectonic history of the Calcatapul Formation, Chubut province, Argentina, and the “Gastre fault system”: *Journal of South American Earth Sciences*, v. 18, p. 73–88, <https://doi.org/10.1016/j.jsames.2004.08.007>.
- Yáñez, G., and Cembrano, J., 2004, Role of viscous plate coupling in the late Tertiary Andean tectonics: *Journal of Geophysical Research: Solid Earth*, p. 109.
- Zaffarana, C.B., and Somoza, R., 2012, Palaeomagnetism and ⁴⁰Ar/³⁹Ar dating from Lower Jurassic rocks in Gastre, central Patagonia: Further data to explore tectonomagmatic events associated with the break-up of Gondwana: *Journal of the Geological Society*, v. 169, p. 371–379, <https://doi.org/10.1144/0016-76492011-089>.

SCIENCE EDITOR: BRAD S. SINGER
ASSOCIATE EDITOR: KAREL SCHULMANN

MANUSCRIPT RECEIVED 30 MAY 2020
REVISED MANUSCRIPT RECEIVED 11 DECEMBER 2020
MANUSCRIPT ACCEPTED 31 JANUARY 2021

Printed in the USA